LIMNOLOGY
and
OCEANOGRAPHY

ASLO

Limnol. Oceanogr. 62, 2017, 2829–2849
© 2017 The Authors Limnology and Oceanography published by Wiley Periodicals, Inc.
on behalf of Association for the Sciences of Limnology and Oceanography
doi: 10.1002/lno.10664

Bloom termination of the toxic dinoflagellate *Alexandrium catenella*: Vertical migration behavior, sediment infiltration, and benthic cyst yield

Michael L. Brosnahan,[1]* **David K. Ralston**,[2] **Alexis D. Fischer**,[1] **Andrew R. Solow**,[3] **Donald M. Anderson**[1]

[1]Biology Department, Woods Hole Oceanographic Institution, Woods Hole, Massachusetts
[2]Applied Ocean Physics and Engineering, Woods Hole Oceanographic Institution, Woods Hole, Massachusetts
[3]Marine Policy Center, Woods Hole Oceanographic Institution, Woods Hole, Massachusetts

Abstract

New resting cyst production is crucial for the survival of many microbial eukaryotes including phytoplankton that cause harmful algal blooms. Production in situ has previously been estimated through sediment trap deployments, but here was instead assessed through estimation of the total number of planktonic cells and new resting cysts produced by a localized, inshore bloom of *Alexandrium catenella*, a dinoflagellate that is a globally important cause of paralytic shellfish poisoning. Our approach utilizes high frequency, automated water monitoring, weekly observation of new cyst production, and pre- and post-bloom spatial surveys of total resting cyst abundance. Through this approach, new cyst recruitment within the study area was shown to account for at least 10.9% ± 2.6% (SE) of the bloom's decline, ~ 5× greater than reported from comparable, sediment trap based studies. The observed distribution and timing of new cyst recruitment indicate that: (1) planozygotes, the immediate precursor to cysts in the life cycle, migrate nearer to the water surface than other planktonic stages and (2) encystment occurs after planozygote settlement on bottom sediments. Near surface localization by planozygotes explains the ephemerality of red surface water discoloration by *A. catenella* blooms, and also enhances the dispersal of new cysts. Following settlement, bioturbation and perhaps active swimming promote sediment infiltration by planozygotes, reducing the extent of cyst redistribution between blooms. The concerted nature of bloom sexual induction, especially in the context of an observed upper limit to *A. catenella* bloom intensities and heightened susceptibility of planozygotes to the parasite *Amoebophrya*, is also discussed.

A prevailing paradigm in the study of microbial eukaryotes is that transitions from asexual reproduction to sexual fusion are induced when a population's environment no longer supports cell division. Sex (and concomitant genetic recombination) enables these cells to replace or repair defective genes during periods when they could not otherwise continue to proliferate. In many species, the sexual process is deeply intertwined with the formation of resting cysts, a life cycle stage that enables survival through sustained periods of poor growth conditions (Margulis et al. 1985). Such life cycle dynamics have been studied extensively among the toxin-producing dinoflagellates that cause harmful algal blooms (HABs) and sexual encystment is frequently cited as a factor contributing to bloom termination (Steidinger 2010). Moreover, the production of new cysts is critical for the persistence and spread of these phenomenon since it is "seed beds" of these cysts that inoculate future blooms (Anderson 1997). Given these roles in HAB dynamics, population genetics, and species biogeography, estimates of the magnitude and dynamics of new cyst production have been long sought.

In laboratory-based investigations, the yield of cysts from batch cultures vary widely, from < 40% to nearly 100% of planktonic precursor stages being converted upon sexual induction through nutrient limitation (Olli and Anderson 2002). Efforts to maximize the yield of culture-formed cysts have explored a wide range of physical and chemical factors including inoculum density, type of macronutrient limitation (nitrogen and/or phosphorus), irradiance intensity, incubation temperature, and salinity (e.g., Anderson et al. 1984; Nagai et al. 2004; Figueroa et al. 2011). Persistent

*Correspondence: mbrosnahan@whoi.edu

This is an open access article under the terms of the Creative Commons Attribution-NonCommercial-NoDerivs License, which permits use and distribution in any medium, provided the original work is properly cited, the use is non?commercial and no modifications or adaptations are made.

questions underlying these efforts have been whether differences in maximum yield reflect variability intrinsic to experimental isolates or suboptimal culture conditions (Coats et al. 1984; Olli and Anderson 2002; Figueroa et al. 2011), and whether production levels observed in the laboratory are ever realized in nature where all life cycle stages are subject to grazing, parasitism, and other forms of mortality.

While measurement of cyst production from cultures is straightforward, its estimation from field populations is challenging because blooms and cyst beds often span large areas (sometimes several thousand km^2) and are spatially patchy in their abundance and degree of sexual conversion (Anderson et al. 2014; McGillicuddy et al. 2014). Several groups have employed sediment traps to estimate the fluxes of new resting cysts (e.g., Garcés et al. 2004; Anglès et al. 2012; Cosgrove et al. 2014) but this approach has known shortcomings including variable capture efficiency and, especially in shallow water systems, contributions from resuspended material that are difficult to constrain (Storlazzi et al. 2010). The use of traps also implicitly assumes that encystment occurs in the water column, but this likely rapid transformation has never been observed in situ (Kokinos and Anderson 1995). The fundamental question of whether encystment occurs in the water column or after bottom settlement therefore remains unresolved. Additional uncertainty is introduced when fluxes are converted to encystment rates because these calculations rely on estimates of the number of planktonic cells in the water, which are again highly uncertain due to their patchiness in space and time (e.g., Rines et al. 2010).

Here, we formulate and apply an alternative, more direct approach to estimate cyst production by a small-scale bloom of *Alexandrium catenella*, a prominent HAB species and the most globally widespread of several dinoflagellates that cause paralytic shellfish poisoning (PSP), a potentially fatal seafood poisoning syndrome. *A. catenella* blooms impact temperate coastal regions along both the east and west coasts of North and South America as well as parts of northern Europe, northwestern Asia, and Africa (Lilly et al. 2007; Anderson et al. 2012; John et al. 2014*a*). Until this year, the species had been called *A. fundyense* or *A. tamarense* Group I where it occurs in the northwest Atlantic (*see* John et al. 2014*a* and references therein). Its naming as *A. catenella* follows a recent adjudication by the Nomenclature Committee for Algae, which found *A. fundyense/A. tamarense* Group I to be synonymous with the earlier described *A. catenella* (John et al. 2014*b*; Fraga et al. 2015; Prud'homme van Reine 2017).

PSP impacts from *A. catenella* arise from blooms that originate in open coastal waters, and from smaller, localized inshore populations (Anderson 1997). These inshore blooms typically are confined within embayments and develop independently from larger coastal blooms, and therefore they are particularly amenable for the study of new cyst production. In this study, intensive manual and automated, in situ observations of one such population in Salt Pond (Eastham, Massachusetts), are leveraged to estimate the peak number of cells and recruitment of new cysts. By combining these estimates, we directly determine the fraction of the planktonic population converted to new diploid resting cysts and deposited within the study area. We also provide evidence of a shift in the vertical migration of *A. catenella* that coincided with the bloom's sexual induction and show that most new cysts were formed after deposition on the pond's bottom.

Methods

Salt Pond study site

Salt Pond is the smallest of three submerged tidal kettle ponds within the Nauset Marsh estuary (Cape Cod, Massachusetts; hereafter referred to simply as Nauset) and has an approximate diameter of 320 m and maximum depth of 9 m. The pond forms the northwest most terminus of the Nauset system and is connected to its other ponds and to the Atlantic Ocean via a central network of shallow marsh channels (Fig. 1). The system's other ponds, Town Cove and Mill Pond, form the southwestern and southern termini, respectively. Nauset tides are semi-diurnal with amplitudes of 1–2 m, and are highly asymmetric, having much shorter floods (3–4 h) than ebbs (8–9 h) (Aubrey and Speer 1985). A consequence of this flood dominance is that net sediment transport is toward Salt Pond and the other terminal ponds.

Each of the three Nauset ponds hosts an independent, localized, and annually recurrent *A. catenella* bloom (Crespo et al. 2011; Fig. 1). Due to the vertical swimming behavior of this species, shallow outlets to the central marsh area, and temperature- and salinity-driven stratification, *A. catenella* cells are largely retained within each pond (Anderson and Stolzenbach 1985; Ralston et al. 2014; Ralston et al. 2015). This retention of cells and north to south gradients in temperature and salinity cause Salt Pond blooms to occur 1–3 weeks later than those to the south (Crespo et al. 2011; Ralston et al. 2014). Thus, the Salt Pond population is isolated from the southern populations in both space and time. Estimates of the total size of the *A. catenella* population within relied on a previously compiled, high resolution model of the pond's bathymetry (Ralston et al. 2015; Fig. 1) and continuous water level measurements from a pressure logger.

Phytoplankton observatory raft operation and water monitoring

A specially-built observatory raft has been deployed within Salt Pond to provide continuous water monitoring data from an Imaging FlowCytobot (IFCB) and other sensors during several *A. catenella* blooms including the focal bloom of this study which occurred in 2013 (Brosnahan et al. 2015). The IFCB is a submersible imaging-in-flow cytometer that captures high quality images of phytoplankton that are 10–100 μm in length at rates of up to 12 s^{-1} (Olson and Sosik 2007). For this study, the IFCB was modified to collect

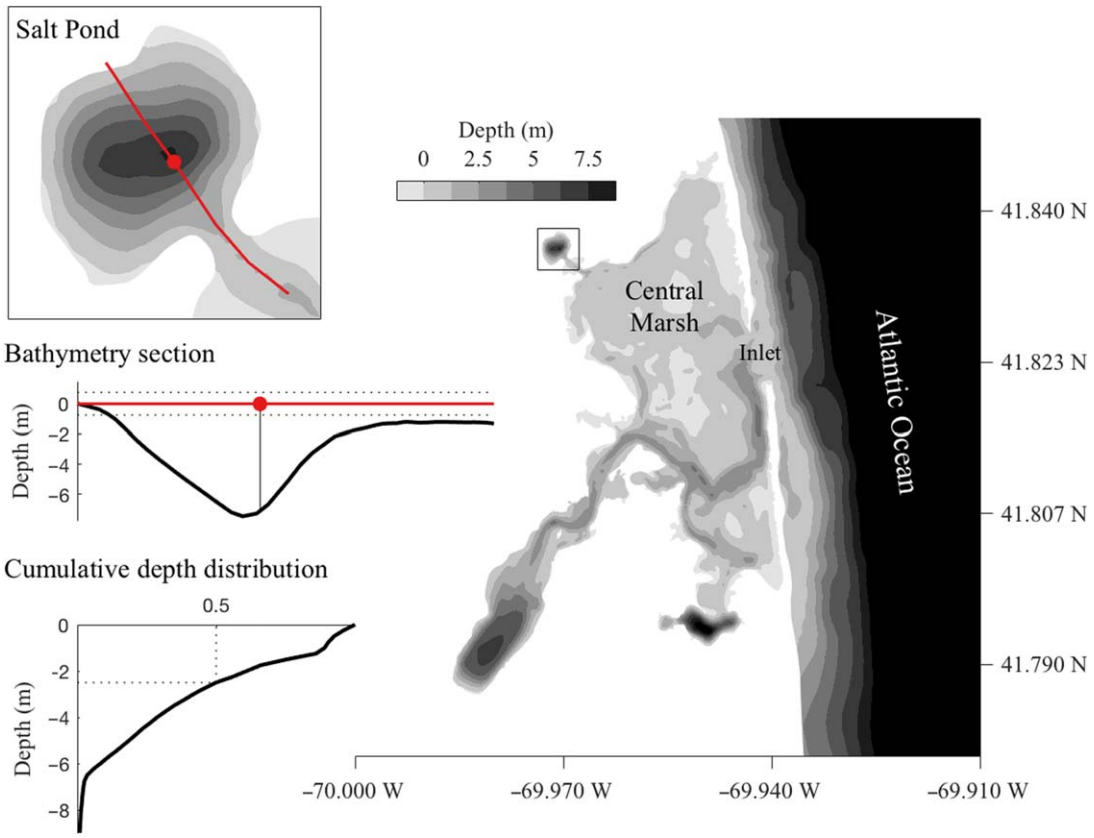

Fig. 1. Bathymetric map of the Nauset Marsh system. Salt Pond is connected to the Atlantic Ocean and other drowned kettle holes within the marsh through a network of shallow channels within a central marsh area. Upper left: Salt Pond bathymetry. The red line indicates a section that passes through the location of the observatory raft (red circle) and is represented in profile in the middle left bathymetry section. Lower left: Cumulative distribution of bottom depths within Salt Pond. About half the pond is ≤ 2 m deep.

samples alternately from two intake ports. Except during step-profiling studies, its two intakes were positioned at depths of 2 m and 5 m, which were the expected day and nighttime depth limits for *A. catenella* vertical migrations (Anderson and Stolzenbach 1985). Sample carryover between depths was minimized by addition of a priming step that flushed > 3 sample volumes of intake water through the instrument's collection syringe prior to collection and analysis of each sample.

An automated winch was also installed on the raft to record profiles of salinity, temperature, chlorophyll *a* fluorescence, and photosynthetically active radiation (PAR) from $\sim$ 1 m to 6 m every 15 min. Profile measurements were made using two conductivity, temperature, and depth (CTD) logging devices: a SeaBird 16plus V2 (SeaBird) and an RBR XR-620 (RBR). The maximum descent rate for this sensor package was less than 7 cm s^{-1}, yielding vertical resolutions of $\sim$ 2 cm. The XR-620 unit was used to measure temperature and conductivity while the 16plus V2 logged measurements from a Seapoint chlorophyll fluorometer (Seapoint Sensors) and irradiance from a QSP-2100 PAR sensor (Biospherical Instruments). Running from their internal batteries in this configuration, the two CTDs could both log continuously at 6 Hz for 6–7 d, but fluorescence profiles were frequently saturated late in the *A. catenella* bloom's development due to a hard-wired gain setting for the SeaPoint sensor. This saturation problem was alleviated during an overnight IFCB step profiling study with an RBR Concerto CTD logger (RBR) that had automatic gain switching, a change that increased the fluorometer's dynamic range threefold.

High quality IFCB observations were collected from 03–20 May, a period that captured the bloom's transition from development to decline and cyst formation. Bloom progression was also monitored through weekly vessel-based surveys that began in early March and included water sampling from the observatory raft at four depths: 1 m, 3 m, 5 m, and 7 m below the surface. Abundance of *A. catenella* from these samples was estimated by epifluorescence microscopy after staining with an *A. catenella* specific ribosomal probe (Anderson et al. 2005; Choi et al. 2017). Subsamples from the same Niskin collections were analyzed for ammonium, nitrite + nitrate, and phosphate concentrations. In the field, these subsamples were filtered through 0.2 μm Sterivex filters, placed on ice for transport, then stored frozen in a -20°C

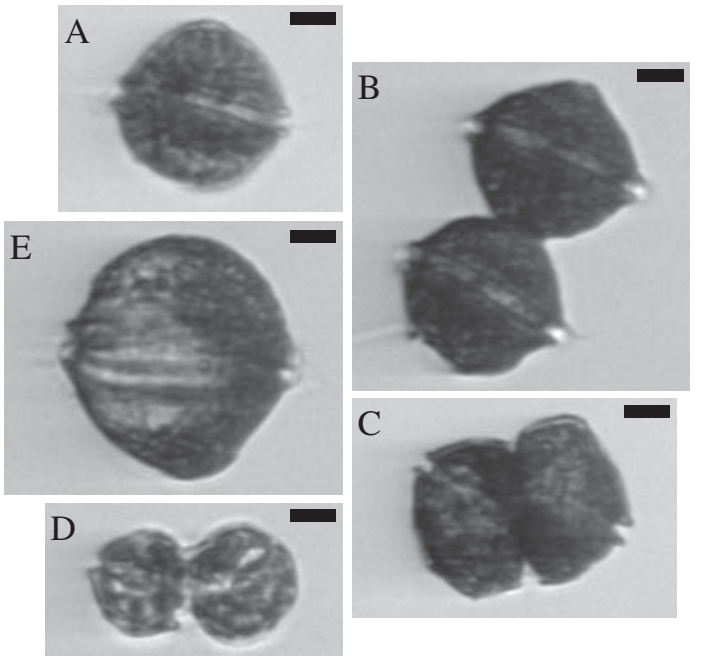

Fig. 2. Representative IFCB images of planktonic *A. catenella* cells. Clockwise from upper left are: (**A**) a vegetative singlet, (**B**) a vegetative doublet, (**C**) dividing cells, (**D**) fusing gametes, and (**E**) a cell with a late stage infection by an *Amoebophrya* parasite. All scale bars are 10 μm in length.

freezer until analysis at the Atlantic Research and Learning Center Laboratory at Cape Cod National Seashore using a 8500 Series QuikChem Flow Injection Analysis system (Lachat Instruments).

Vertical step profiling studies with the IFCB

To better characterize the vertical distribution of the different *A. catenella* life cycle stages, two IFCB step profiling studies were conducted: one overnight study that coincided with the bloom's transition from vegetative cell to gamete dominance (08–09 May) and a second daytime study that coincided with transition to planozygote dominance (13 May). During both studies, IFCB sampling was monitored in real time on site and the depth of the instrument was cycled every 1.5 h through 1-m steps at the near surface and 1 m, 2 m, 3 m, 4 m, and 5 m depths using a hand winch. For the overnight study, five additional Niskin bottle profiles of *A. catenella* abundance and nutrient concentrations were collected every 6 h (at 12:00 h and 18:00 h, 08 May; and 00:00 h, 06:00 h, and 12:00 h, 09 May).

***A. catenella* image classification and analysis**

Images of *A. catenella* from the IFCB had to be identified and sorted into life cycle stage types and other ecologically relevant classes (Fig. 2). This classification task was undertaken with three major objectives in mind: (1) characterization of the timing and extent of the *A. catenella* bloom transition from dividing vegetative cells to its sexual stages, (2) estimation of the total abundance and biovolume of *A. catenella*, especially at the peak of its bloom, and (3) rigorous assessment of the relative abundance and frequency of *A. catenella* sexual stages, particularly fusing gamete pairs and late stage planozygotes.

To meet these objectives, a two-step classification scheme was applied that took advantage of a suite of MATLAB-based IFCB image classification software (Sosik and Olson 2007; https://github.com/hsosik/ifcb-analysis) and a previously constructed and characterized random forest based classification machine (Brosnahan et al. 2015). The classification machine was built from training images collected during a Salt Pond *A. catenella* bloom in 2012 and includes two *A. catenella* "subclasses" for singlet and doublet cells and 40 additional species- and genus-level classes corresponding to commonly co-occurring dinoflagellates, diatoms, and ciliates. The two-subclass classifier is both more sensitive and specific for *A. catenella* than similar classifiers that attempt to sort all *A. catenella* into a single class or a more comprehensive list of subclasses. Size dynamics within the singlet subclass also indicate the timing and extent of life cycle transitions. Specifically, vegetative populations are characterized by diel oscillations in mean singlet cell volume that are associated with phased division; gametogenesis by conversion of the population to small, gamete cells that are exclusively involved in cell-cell fusions; and zygosis by singlets that are similar in size to vegetative cells but whose mean volume grows monotonically over a period of several days.

Accurate assignment of other *A. catenella* classes including three- and four-cell chains, those with mature grade infections by *Amoebophrya* parasites, dividing cells, fusing gametes, and new resting cysts required manual inspection and reassignment of *A. catenella* images from the two machine-assigned subclasses. All IFCB samples collected from 07 May to 13 May were manually reviewed and *A. catenella* images sorted among the comprehensive set of subclasses because this period spanned the last days of the bloom's development, its peak, and a sustained gametic phase that lasted from 09 May to 13 May. Manual review was periodic on a subset of the samples collected prior to and after this period. Assessments of total abundance accounted for differences in cell number between subclasses (e.g., vegetative doublets, dividing cells, and fusing gametes were each counted as two cells). Frequencies of fusing gametes and late-stage planozygotes were calculated in relation to these corrected abundances. Biovolume estimates for *A. catenella* and other taxa in each sample were determined using a distance map approach that is incorporated within the IFCB classification software suite (Moberg and Sosik 2012).

Progression of sexual stages toward encystment was assessed from IFCB-based frequency measurements. First, the question of whether frequencies of sexual stages varied with

depth was examined through comparisons of stage frequencies above, within, and below the depth of the chlorophyll maximum. Similarly, variability associated with time of day was explored by reviewing stage frequencies between 07 May and 13 May, the period when sexual stages were most abundant and when all observations were corrected and sorted into subclasses from the comprehensive set. Finally, the duration of gamete fusion (t_{fus}) was estimated from the frequency of fusing cells, using the relationship:

$$t_{\mathrm{fus}} = \frac{T_{\mathrm{fus}}}{n \cdot \ln(1+F_{\mathrm{fus}})} \sum_{i=1}^{n} \ln(1+f_i) \quad (1)$$

where T_{fus} is the duration of the period when fusion (but not division) was occurring (09–13 May), F_{fus} is the fraction of the population undergoing fusion, and f_i is the frequency of fusing gametes observed during each of n IFCB observations made during T_{fus}. The equation is adapted from one used to estimate rates of mitotic division (Chisholm and McDuff 1982) under the assumptions that gamete fusion is irreversible and that gametes, planozygotes, and all other life cycle stages experienced equal loss rates from the pond. This calculation was compared to direct laboratory measurements to assess both the extent of fusion and the validity of the calculation.

Estimation of peak abundance of planktonic life-cycle stages

Because *A. catenella* was the dominant species recorded by the IFCB in the days near the peak of its bloom, chlorophyll fluorescence profiles were assessed to determine whether they accurately described cells' vertical distribution and abundance. IFCB-based biovolume estimates were aligned to fluorescence measurements made during the 08–09 May and 13 May IFCB step profiling studies (periods when profiles were minimally affected by sensor saturation and when IFCB observations were most evenly distributed across the full depth range of the population). Alignment of fluorescence and biovolumes was optimized across profile segments of 0.1–0.9 m and IFCB intake positions fixed within 0.25 m of their nominal depth. Optimization was based on correlation coefficients from the regression model:

$$\ln B = \hat{\beta}_0 + \hat{\beta}_1 \ln F \quad (2)$$

where $\hat{\beta}_0$ and $\hat{\beta}_1$ are the estimated parameters from a regression of biovolume (B) against the fluorometer measurement (F) for the sample of paired biovolume and fluorescence measurements. Regressions were assessed and compared to similar fits of fluorescence to biovolume of all images not classified as *A. catenella*. Finally, residuals from fits of *A. catenella* biovolume and chlorophyll fluorescence were inspected for temporal and depth-based trends.

Conversion of fluorescence profiles to estimates of total *A. catenella* abundance applied the regression between fluorescence and *A. catenella* biovolume and also took into account the study site's bathymetry and tidal water level. Our approach assumes that fluorescence profiles provide an unbiased estimate of the mean cell concentration at any given depth across the pond. Though not tested directly in this study, no such bias was observed during high frequency spatial surveys of chlorophyll fluorescence that coincided with intense phases of Salt Pond *A. catenella* blooms in 2011 and 2012. The earlier surveys demonstrated strong spatial coherence in the depth of the chlorophyll maximum near the peak of *A. catenella* blooms, particularly during tide ebbs. During floods, incoming water mixed fluorescence near the entrance to the pond downward and pushed high fluorescence layers toward the pond's periphery (Ralston et al. 2015; unpubl. data). Integrals of total *A. catenella* biovolume in the pond took into account the water level at the time of each profile using the bathymetry of the pond and linearly interpolated *A. catenella* biovolume from the profile limits ($\sim$ 1 m and 6 m) to the pond's surface and bottom, assuming 0 biovolume at these boundaries. Total *A. catenella* biovolume was then converted to cell abundance using contemporaneous IFCB observations of mean cell volume. This hypsometric correction procedure took into account an expected dilution effect whereby the cell population would tend to decrease in concentration when cells occupy shallower depths (i.e., where a greater fraction of the pond's total volume is distributed, Fig. 1). The resulting estimates were compared to simple estimates made from means of cell concentrations observed in Niskin collections from the raft taken 08 May, 09 May, and 13 May.

More formally, to estimate total *A. catenella* abundance, $\hat{T}$, and its uncertainty, individual fluorescence profiles were considered as samples of unit volume taken along a sequence of depths at a single location in the pond (the observatory raft). The estimated cell number at a single time is given by:

$$\hat{T} = \sum_{d=1}^{D} w_d e^{\hat{\beta}_0} {F_d}^{\hat{\beta}_1} \quad (3)$$

where w_d is the product of the conversion factor from biovolume to cell number and total volume within depth bin d and F_d is the fluorometer measurement for a unit volume for depth bin d. The standard error of $\hat{T}$ can be approximated classically by:

$$\mathrm{SE}\left(\hat{T}\right) \cong \sqrt{\delta' \Sigma \, \delta} \quad (4)$$

where $\delta = \left(\frac{\partial \hat{T}}{\partial \hat{\beta}_0} \; \frac{\partial \hat{T}}{\partial \hat{\beta}_1} \; \frac{\partial \hat{T}}{\partial F_1} \ldots \; \frac{\partial \hat{T}}{\partial F_D}\right)'$ where $'$ denotes transpose and Σ is the $(D+2)$-by-$(D+2)$ covariance matrix of $\hat{\beta}_0$, $\hat{\beta}_1$, F_1, …, F_D. The elements of the vector δ are approximated by:

$$\frac{\partial \hat{T}}{\partial \hat{\beta}_0} \cong \hat{T} \tag{5}$$

$$\frac{\partial \hat{T}}{\partial \hat{\beta}_1} \cong e^{\hat{\beta}_0} \sum_{d=1}^{D} w_d \; F_d{}^{\hat{\beta}_1} \tag{6}$$

$$\frac{\partial \hat{T}}{\partial F_d} = w_d e^{\hat{\beta}_0} \hat{\beta}_1 \; F_d^{\hat{\beta}_1 - 1} \tag{7}$$

Covariances of $\hat{\beta}_0$ and $\hat{\beta}_1$ are taken from standard regression outputs and covariances of $F_1, \ldots, F_D$ are calculated from fluorescence profiles collected within a 2-h moving window of each point estimate under the assumption that individual casts are independent. Finally, the covariance of the regression estimates ($\hat{\beta}_0$ and $\hat{\beta}_1$) and the fluorometer measurements used to form $\hat{T}$ are 0. This ensures that the variance of $\hat{T}$ can be decomposed into the sum of a term that depends only on the variances and covariance of the regression estimates and a term that depends only on the variances and covariances of the fluorometer measurements.

An estimate of the peak number of planktonic cells is made by averaging point estimates from casts collected within 2 h of the end of the morning division period of 09 May. Exploiting the decomposition described above, we approximate the variance of this averaged estimate by the sum of the term depending only on the variability of the regression estimates evaluated at the mid-point of this interval and the average over this interval of the terms depending only on the variability of the fluorometer measurements further divided by 8 (the number of casts averaged). This approximation assumes that the fluorometer measurements at different sampling times within this interval are uncorrelated. This assumption was verified by examining the time series of fluorometer measurements at each depth within the averaging interval.

Weekly time series of new resting cyst deposition

The timing and extent of new cyst deposition was examined using two different approaches. The first was deployment of tube traps 4 m below the observatory raft. Traps consisted of four cylindrical tubes, each 60 cm long and 10.5 cm in diameter, that were secured to a cross-shaped frame. Tube openings were fitted with a 2-cm thick baffle to reduce turbulence and improve trapping efficiency. Prior to deployment, traps were pre-filled with 0.2 μm filtered seawater that was underlain with a heavy poison solution (5% unbuffered formalin in seawater [v/v], adjusted to 1.034 g mL^{-1} by sodium chloride addition) to a height of 10 cm. Filled traps were carefully lowered from the raft to minimize disturbance and recoveries and redeployments occurred approximately weekly. Upon recovery, trap contents were stored on ice for transport then stored at 4°C until laboratory analysis within 1 week of collection.

Captured material was disaggregated by sonication then passed through a series of Nitex sieves to isolate the cyst-containing 20–100 μm size fraction for staining with primulin as described by Yamaguchi et al. (1995). Briefly, 20–100 μm fractions were fixed in 10% unbuffered formalin in seawater (v/v) at 4°C for at least 30 min, then resuspended in −20°C methanol for pigment extraction (at least 48 h). Cyst fractions were then resuspended in 200 μg mL^{-1} primulin in deionized water and allowed to stain for 30 min at room temperature before rinsing with deionized water and counting under a Zeiss Axioskop microscope with blue light excitation and a 520 nm long pass emission filter. *A. catenella* cysts were identified by positive staining and their characteristic pill shape, 55–60 μm long and 20–25 μm in diameter. The contents of at least 3 of the 4 traps deployed each week were counted. Capture rates are expressed as the mean number of cysts collected per trap divided by the number of days the trap was deployed. No effort was made to convert trap collections directly to deposition rates since captured particles reflected both newly deposited and resuspended material.

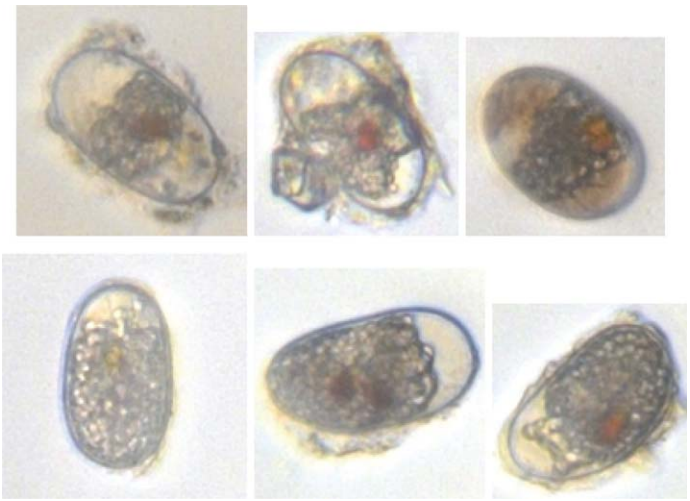

Fig. 3. Images of matured (top row) and new resting cysts (bottom row).

A second approach for determining the timing and extent of new cyst deposition was direct observation of new cysts in surface sediment samples. Immediately after their formation, the cytoplasm of new *A. catenella* cysts is filled with starch granules that are consumed and become concentrated around the cysts' mid-body or poles as cysts mature, a process that takes 1–3 months (Fig. 3; Anderson 1980). Using this morphological distinction, the abundance of new cysts was recorded relative to the older mature ones. Triplicate cores were collected from a boat in shallow water (< 1 m deep) near the pond's northern shore during weekly surveys. On site processing included aspiration of headwater and extrusion to collect the 0–1 cm layer of uppermost sediment. This mud was stored on ice for transport to the laboratory where it was disaggregated by sonication and enriched by

sieving as previously described. Cysts were further enriched from sediment using density cushion centrifugation as described by Schwinghamer et al. (1991). The dense, cushion solution for this enrichment was prepared from a Nalco 1060 base with sucrose added to achieve initial densities of > 1.38 g mL^{-1}. Cysts were removed from the cushion/sediment suspension interface, then washed over a 20 μm Nitex sieve with 0.2 μm filtered seawater before examination under 160X magnification. The concentration of cysts cm^{-3} wet sediment and the new : old ratio were determined from observation of no less than a sum of 449 new and old cysts across all cores taken each week.

Similar sediment analysis was undertaken before and after new cyst production by a Salt Pond bloom in 2016 with the goal of characterizing the timing and extent of new cyst appearance in both the surface (0–1 cm) and subsurface (1–3 cm) sediment layers. This later sampling effort examined new cyst deposition both at the northern shore and at sites immediately outside of Salt Pond.

Spatial surveys of resting cyst abundance in Salt Pond

To estimate the total deposition of new resting cysts, three spatial surveys of cyst abundance were conducted. The first, a pre-bloom survey was completed 19 November 2012; the second, a post-bloom survey 17 and 18 July 2013; and the third, a follow-up post-bloom survey 15 November 2013. During each survey, single sediment cores were collected at 22–42 evenly distributed stations. Processing and analysis of cores was similar to those collected during weekly surveys but no effort was made to differentiate new and old cysts. Cores were extruded for collection of the uppermost 0–1 cm surface and the 1–3 cm subsurface layers on site. Abundance estimates were made from observations of more than 400 primulin-stained cysts or a maximum of 0.1 cm^3 raw sediment analyzed, whichever represented a smaller subsample (Anderson et al. 2003).

Estimates of total cyst abundance and cyst yield

To estimate total cyst number, log cyst density was projected onto a regular spatial grid, transformed to the linear scale, and integrated over the grid locations. The approach is based on an explicit statistical model from which the standard error of estimated total cyst abundance can be calculated. Specifically, let $\rho(x)$ be cyst density at location x within the pond. Our basic statistical model is:

$$\log \rho(x) = \mu(x) + \varepsilon(x) \tag{9}$$

where $\mu(x)$ is a smoothly varying spatial trend and $\varepsilon(x)$ is a spatially uncorrelated normal error with variance σ^2 that reflects a combination of measurement error and natural variability in cyst density (i.e., patchiness). The allowance for a spatial trend is important in characterizing the uncertainty of total cyst number. In particular, assuming a constant error in the presence of a spatial trend will attribute variability due to the trend to error and inflate the standard error of total cyst number. The estimate of the spatial trend at grid location x is:

$$\hat{\mu}(x) = \sum_{j=1}^{n} w_j(x) \log \rho(x_j) / \sum_{j=1}^{n} w_j(x) \tag{10}$$

where $\rho(x_j)$ is the measured cyst density at sampling location x_j and the weight on this measurement in estimating log density at location x is:

$$w_j(x) = \exp\left(-0.5 \left(\frac{|x - x_j|}{h}\right)^2\right) \tag{11}$$

where h is a bandwidth that controls the smoothness of the spatial trend. This is a standard application of Gaussian kernel estimation. Technical details are provided in Hastie and Tibshirani (1990). The bandwidth selected by least squares cross-validation was 35 m. The error variance σ^2 was from the sample values as:

$$\hat{\sigma}^2 = \sum_{j=1}^{n} \left(\log \rho(x_j) - \hat{\mu}(x_j)\right)^2 / (n - \mathrm{df}) \tag{12}$$

where df is the effective degrees of freedom of the kernel estimate.

The estimate of cyst density is given by:

$$\hat{\rho}(x) = \exp\left(\hat{\mu}(x) + \frac{\hat{\tau}^2(x)}{2}\right) \tag{13}$$

where:

$$\hat{\tau}^2(x) = \hat{\sigma}^2 \frac{\sum_{j=1}^{n} w_j^2(x)}{\left(\sum_{j=1}^{n} w_j(x)\right)^2} \tag{14}$$

is the estimated variance of $\hat{\mu}(x)$. Finally, the estimate of total cyst number is found by summing the values of $\hat{\rho}(x)$ across the grid points, denoted by g_k, $k = 1, 2, \ldots, K$. The estimate $\hat{\rho}(g_k)$ of cyst density at g_k is given in Eq. 13 above. The estimate of total cyst number is:

$$\hat{C} = a \sum_{k=1}^{K} \hat{\rho}(g_k) \tag{15}$$

where a is the area of a grid cell. The standard error of $\hat{C}$ is the square root of its variance, which can be approximated as:

$$\mathrm{Var}\ \hat{C} \cong a^2 \sum_{k=1}^{K} \sum_{l=1}^{K} \hat{\rho}(g_k) \hat{\rho}(g_l) Cov(\hat{\mu}(g_k), \hat{\mu}(g_l)) \tag{16}$$

where:

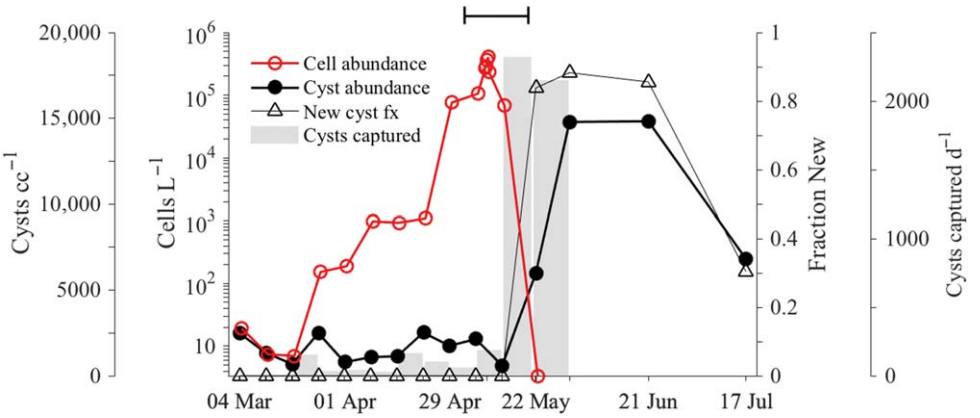

Fig. 4. Measures of bloom progression and new cyst deposition made through weekly water and sediment sampling. Cell concentrations (red) are means of bottle samples collected at 1 m, 3 m, 5 m, and 7 m. Cyst abundance and new cyst fractions (closed black circles and open black triangles, respectively) are means of triplicate sampling of surficial sediment (0–1 cm layer) near the northern shore of Salt Pond. Cyst capture rate by tube traps deployed at 4 m depth is plotted in gray bars. The final sediment trap deployment ended 31 May. The capped line (top) spans the IFCB observation period.

$$\mathrm{VCov}(\hat{\mu}(g_k),\ \hat{\mu}(g_l)) = \frac{\hat{\sigma}^2 \ \sum_{j=1}^{n} w_j(g_k) w_j(g_l)}{\sum_{j=1}^{n} w_j(g_k) \ \sum_{j=1}^{n} w_j(g_l)} \tag{17}$$

and where $\hat{\sigma}^2$ is given in Eq. 12 and, as above:

$$w_j(g_k) = \exp\left(0.5 \left(\frac{|x_j - g_k|}{h}\right)^2\right) \tag{18}$$

Because new cysts were found to be proportionally dominant in both the 0–1 cm surface and 1–3 cm subsurface sediment layers, total new cyst deposition is estimated as $p_{\mathrm{new}}\hat{C}_X$, where $\hat{C}_X$ is the estimated number of cysts present during the July post bloom survey and p_{new} is the peak fraction of new cysts observed in the cyst morphology time-series. In turn, cyst yield, $\hat{Y}$, is estimated:

$$\hat{Y} = \frac{2 p_{\mathrm{new}} \hat{C}_X}{\hat{T}} \tag{19}$$

where the factor 2 accounts for the production of cysts from the fusion of two gamete cells. Uncertainty in the estimate of cyst yield is approximated via the expression:

$$\mathrm{SE}\left(\hat{Y}\right) \cong 2\frac{p_{\mathrm{new}}\hat{C}_X}{\hat{T}} \sqrt{\frac{\mathrm{SE}\left(p_{\mathrm{new}}\hat{C}_X\right)^2}{{p_{\mathrm{new}}\hat{C}_X}^2} + \frac{\mathrm{SE}\left(\hat{T}\right)^2}{\hat{T}^2}} \tag{20}$$

where $\mathrm{SE}\left(p_{\mathrm{new}}\hat{C}_X\right)$ and $\mathrm{SE}\left(\hat{T}\right)$ are the standard errors of $p_{\mathrm{new}}\hat{C}_X$ and $\hat{T}$ (from Eqs. 4, 16).

Results

Bloom progression and timing of new cyst formation

A. catenella vegetative cells were present in Salt Pond from the first sampling survey 04 March 2013 but mean concentrations did not exceed 1000 cells L^{-1} until 22 April. Concentrations then rose monotonically until the peak on 09 May (Fig. 4). The greatest cell concentration observed in Niskin bottle sampling exceeded 1×10^6 cells L^{-1} (taken shortly after 00:00 h, 09 May), and while concentrations observed by IFCB were similar on average, the peak IFCB concentration was greater (8.19×10^6 cells L^{-1}, 02:45, 09 May). After the peak of the bloom, up to 80% of *A. catenella* transformed to small gametes (Fig. 5). At this time, cyst concentrations from cores remained approximately constant (mean 770 cysts cc^{-1}) and none had new morphology. Background capture of resuspended cysts in tube traps positioned 4 m below the observatory raft was consistently $\sim$ 100 resting cysts d^{-1} throughout this period (04 March–06 May; Fig. 4).

From 09 May 2013 to 13 May 2013, mean concentrations from Niskin bottle profiles fell about fourfold (from 403,000 to 103,000 cells L^{-1}) but cyst abundance in cores and cyst capture by the tube trap were unchanged. Nine days later (22 May), mean cell concentration dropped to near 0 (3.8 cells L^{-1}) and cyst concentration increased significantly (unpaired *t*-test, $p < 0.01$) by nearly eightfold to 5990 cysts cc^{-1}, and 84% had new morphology. The number of cysts captured by the tube traps jumped markedly as well, to 2320 cysts d^{-1} (a 23-fold increase). The transition from bloom development to decline was not obviously attributable to limitation by nitrogen or phosphorus as mean concentrations were slightly higher through the bloom's transition to its sexual phase than during its development (6.59 μM, 0.49 μM, and 0.69 μM NH_4^+, $NO_2^- + NO_3^-$, and PO_4^{-3}, respectively, during termination and 5.89 μM, 0.09 μM, 0.97 μM NH_4^+, $NO_2^- + NO_3^-$, and PO_4^{-3} during development).

Cyst concentrations in sediment increased an additional 2.5-fold (to 14,780 cysts cc^{-1}) when sampled 9 d later (31

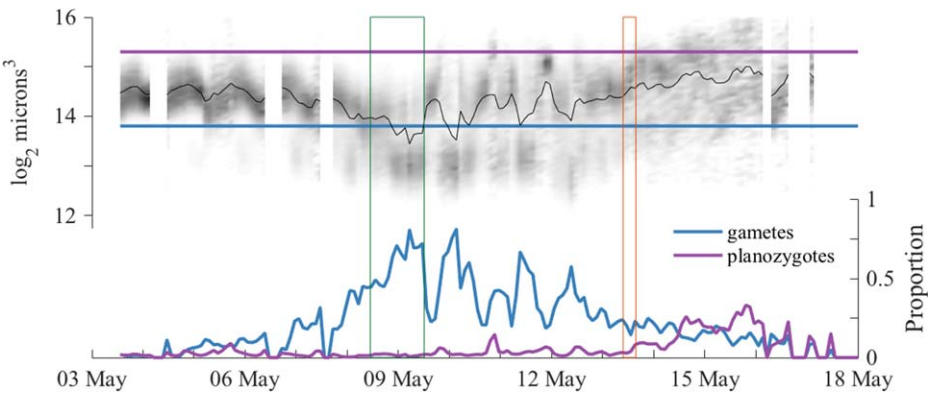

Fig. 5. *A. catenella* singlet size dynamics and partitioning of the population into gamete and mature planozygote size classes. Green and orange rectangular outlines denote intervals when IFCB step-profiling studies were conducted. Upper panel: Singlet cell volume distribution is presented as a gray scale histogram at each sample time. Darker shades represent a larger proportion of cells having the given size than lighter shades. These size dynamics are overlain by the 2-h moving window mean of cell volume (black line). Horizontal lines defining gamete and planozygote size thresholds are drawn in blue and purple, respectively. Bottom panel: Partitioning of the *A. catenella* population into gamete and mature planozygote size classes.

May 2013; unpaired *t*-test, $p = 0.001$), a period when *A. catenella* was essentially absent from the water column. The proportion of cysts that were new increased slightly to 88%. Daily capture rate by tube traps at 4 m was unchanged from the prior sampling period (mean 2150 cysts d^{-1}). No additional water samples were collected after the 31 May and sediment sampling was suspended until a spatial survey of all cysts was completed 7 weeks later (17 and 18 July 2013).

IFCB-based assessments of life cycle transitions

Sampling by the IFCB from 03 May 2013 to 20 May 2013 successfully recorded transitions from a population dominated by vegetative cells to one dominated by gametes and then planozygotes. Though pairs and higher-number chains were commonly recorded, the majority *A. catenella* were singlets (> 90% of images in all samples), which was advantageous for assessment of life cycle transitions from singlet cell size dynamics.

From 03 May to 08 May, the population was dominated by vegetative cells as evidenced by diel oscillations in mean cell volume (associated with phased mitotic division during early morning hours; Fig. 5). Gamete-sized cells (< 14,260 μm^3) and gamete-gamete fusions were also observed during this period but were rare and thus the earliest sexual fusions did not prevent continued population growth. In the early morning hours 08 May, the population began mass conversion to small gamete-sized cells and reached peak gamete fractions of 80.7% and 81.2% early on 09 May and 10 May, respectively (Fig. 5). Between these peaks, a greater than fourfold decline in both the abundance of total cells and the gamete fraction coincided with a daytime flood tide, as the water flowing into the pond temporarily displaced the gamete population to the pond's periphery and brought with it lower concentrations of comparatively large *A. catenella* cells (most likely young planozygotes). This pattern was repeated during the morning flood 10 May when the gamete fraction fell from 60% to 20%, then rose back to 43% late in the following ebb, and again during daytime floods 11 May and 12 May. Planozygotes recorded during the 12 May flood were heavily infected by the intracellular parasite *Amoebophrya* (up to 44%; Figs. 2, 6). From 13 May until the demise of the bloom, daytime floods were no longer associated with oscillations in the gamete fraction but were enriched with larger, infected planozygotes, reaching peak fractions of 29%, 33%, and 32% on 13 May, 14 May, and 15 May, respectively.

Gamete-gamete fusions were observed in most samples from 09 May 2013 to 13 May 2013, including 73% of samples collected from the shallow intake and 49% at the deep intake. After 13 May, when planozygotes and infected cells were increasingly prevalent, fusions were much less common (observed in 6% of samples). The duration of fusion estimated from observed frequencies through the 09–13 May period ranged from a minimum of 2 h if all cells fused (i.e., $F_{fus} = 1$) to > 14 h if only 10% did ($F_{fus} = 0.1$; Fig. 7). With ~ 80% being converted to new planozygotes (from the maximum gamete fraction observed on 09 May), the duration of fusion was estimated to be 2.4 h.

A second estimate of the duration of gamete fusion was made through assessment of the fusing gametes' depth distribution. The frequency of fusing gametes relative to other life cycle stages was enriched above the chlorophyll maximum (Fig. 8; unpaired *t*-test, $p < 0.001$), but lacked any diel pattern. The greatest absolute concentration of fusions occurred 0.6 m above the chlorophyll maximum (70 mL^{-1}, 01:25 h, 09 May) and greatest mean concentrations were between 0.4 m and 0.8 m above it. Under the assumptions that most initial gamete encounters occurred at the chlorophyll maximum (where their concentration was greatest) and that paired cells swam upward at a speed similar to observed rates of vertical migration (0.6–0.8 m h^{-1}), the duration of fusion was < 1 h.

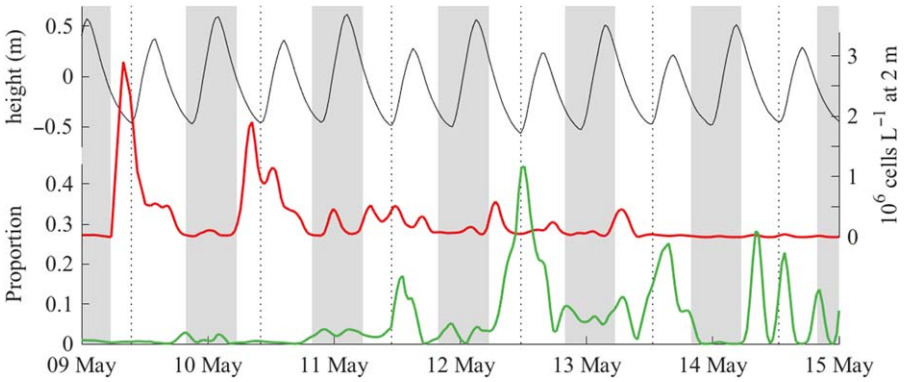

Fig. 6. Association of daytime flood tides with drops in cell abundance detected by the IFCB at 2 m below the pond's surface (red line, right vertical axis) and spikes in the prevalence of mature *Amoebophrya* infections (green line, lower left vertical axis). Nighttime periods are indicated by vertical gray bars and dotted rules mark the timing of daytime low tides. Water level (black line) is plotted against the upper left vertical axis.

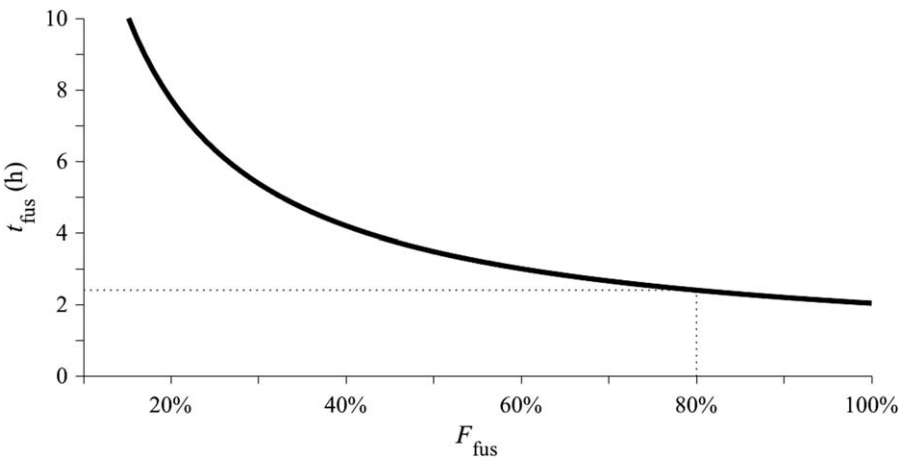

Fig. 7. Estimates of the duration of gamete fusion (t_{fus}) derived from observed fusion frequencies and calculated across a range of population fractions that might have formed zygotes (F_{fus}). The value of t_{fus} at $F_{fus} = 0.8$ (approximately the proportion of the Salt Pond population that formed gametes 09 May) is 2.4 h and is marked by dotted guidelines.

Late stage planozygotes, defined as cells larger than 40,340 μm^3 (Brosnahan et al. 2015), were also detected throughout the IFCB observation period but did not represent a sizeable fraction until after 13 May (when the bloom had largely dissipated). Unlike during the 09–13 May period, changes in planozygote frequency and concentration were not associated with tidal floods but spatially they were enriched ~ 2-fold above the chlorophyll maximum (unpaired *t*-test, $p < 0.001$), similar to fusing gametes (Fig. 8).

A total of 89 new resting cysts were also observed by the IFCB, the first on 10 May and the last on 16 May. The total number in any one IFCB sample never exceeded four cysts (< 2.5 mL per sample, < 15 mL h^{-1}). Capture of new cysts by the IFCB was biased toward the shallow intake (at or above 2 m depth; 63%) and during flood tides (62%) even though floods represented only about a third of the total samples collected and manually classified.

Estimates of total planktonic population size

A. catenella cells were the dominant contributor to total observed fluorescence (and therefore also the chlorophyll maximum layers) throughout the 08–13 May 2013 period (*F*-test, $p < 0.001$; Fig. 8). Residuals from regression of the aligned fluorescence and biovolume measurements were clustered around 0 through the day–night cycle, indicating no change in fluorescence per unit biovolume. Fluorescence profiles were therefore directly interpretable as maps of *A. catenella* abundance through the water column and were characterized by a well-defined thin layer, especially during tide ebbs (Fig. 8). Migration of this layer occurred predictably around dawn and dusk throughout the bloom's development phase, moving at 0.6–0.8 m h^{-1} between ~ 5 m overnight and ~ 2.5 m during the day. After the bloom's gametic transition (09 May), ambits became progressively shallower each day so that cells swam only to 3.25 m depth

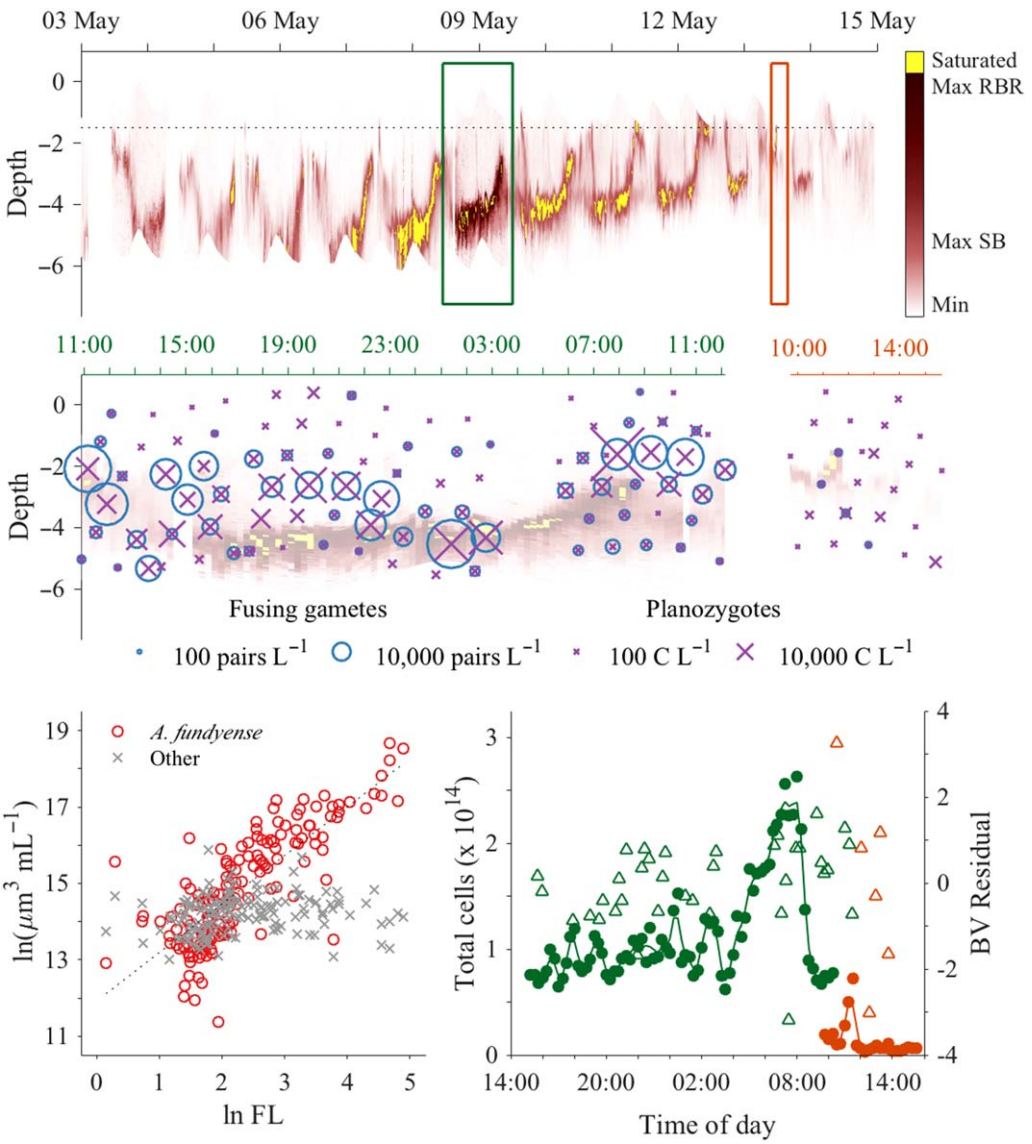

Fig. 8. Profiles of chlorophyll fluorescence and alignment to IFCB observations. Top axes: Time series of fluorescence profiles captured every 15 min through the late stages of the *A. catenella* bloom's development and its termination. Maximum fluorescence values measurable by the two CTD loggers used are indicated on the colorbar (Max SB and Max RBR, respectively). The alternate RBR logger increased the dynamic range of the fluorometer during the overnight study, reducing the incidence of saturation relative to periods immediately before and after. A dotted black line marks the maximum depth of the outlet channel from Salt Pond. Intervals of two IFCB step profiling studies, one overnight at the bloom's peak and one daytime study during its termination, are marked by green and orange rectangular boxes, respectively. Middle axes: Concentration estimates of fusing gamete pairs and mature planozygotes during IFCB step profiling studies. Data are superimposed on the chlorophyll fluorescence profile time series. Data from the overnight study are presented along the left (green) time axis (11:00–12:00 h) and data from the daytime study are presented along the right (orange) time axis (10:00–15:00 h). Bottom left: Comparison of aligned fluorescence and IFCB cell biovolume estimates. *A. catenella* biovolume was strongly correlated with measured fluorescence while biovolume of all other cell types combined was not. Bottom right: Estimates of total *A. catenella* cell abundance within Salt Pond calculated from fluorescence profiles during the bloom peak (green closed circles) and termination phase (orange close circles) profiling studies are plotted against the left vertical axis. Residuals from linear regression of aligned, log-transformed fluorescence and IFCB-based biovolume estimates (green and orange open triangles) are plotted against the right vertical axis.

overnight 13–14 May while daytime upper bounds were shallower than 1 m below the surface and no longer observable by our profiler.

Estimates of the total population from fluorometer profiles were remarkably stable at around 1×10^{14} cells within the confines of Salt Pond through the first 19 h of the overnight profiling study (08–09 May; Fig. 8). Beginning at 04:00 h on 09 May, estimates of total *A. catenella* population size increased to $> 2 \times 10^{14}$ cells, a surge that coincided with the population's morning ascent as well as a drop in the

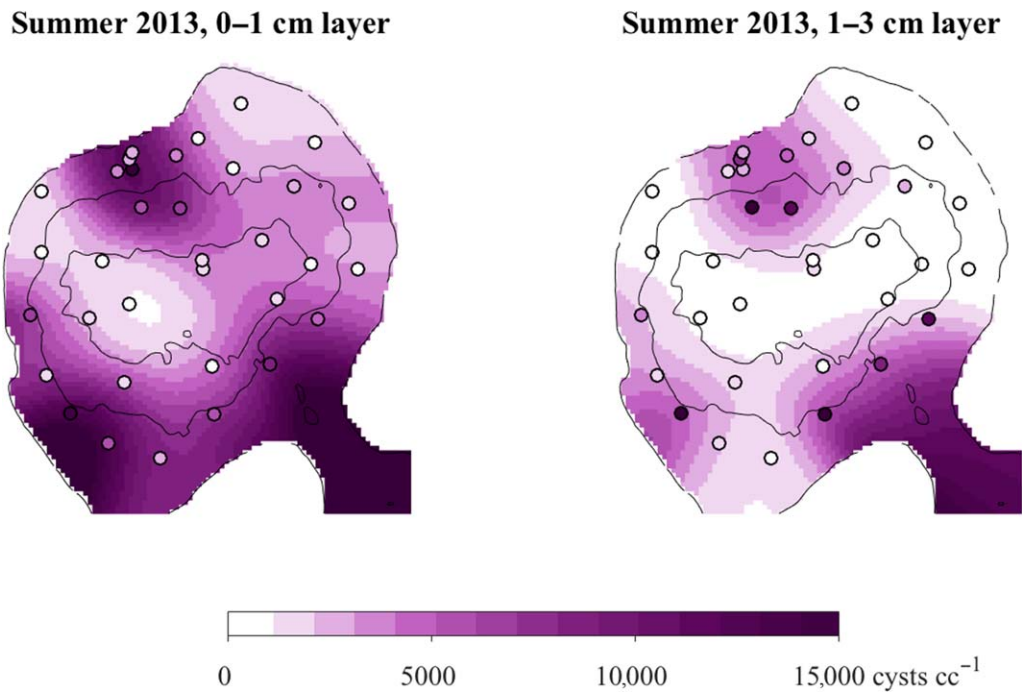

Fig. 9. Observed and interpolated surface (0–1 cm) and subsurface (1–3 cm) cyst abundances, July 2013. Observations from sediment cores are marked by open circles that are colored from white to purple according to recorded abundances. Interpolated concentrations are shaded on the same color scale. Black contours mark depths of 2.5 m and 5 m, the approximate limits of vertical migration by planktonic vegetative cells.

mean cell volume, indicating a phased division (Figs. 5, 8). Beginning at 08:30 h on 09 May when cells had reached the upper limit of their ambit (2.5 m depth) and the flood tide began, estimates fell to $< 1 \times 10^{14}$ cells due to displacement to the pond's periphery by water coming in from the inlet channel. Coarser estimates derived from Niskin bottle sampling were somewhat lower: 7.6×10^{13}, 7.9×10^{13}, 1.0×10^{13}, 1.1×10^{13}, and 0.64×10^{13} cells from profiles collected 08 May at 12:00 h and 18:00 h and 09 May at 00:00 h, 06:00 h, and 12:00 h, respectively.

Two sources of error in the individual fluorometer-based estimates of the total planktonic population size were considered, uncertainty in linear regression parameters and patchiness in the spatial distribution of cells. Variance due to spatial patchiness, assessed through comparison of profiles collected within a 2-h moving window, was the more significant of these for individual point estimates ($\sim$ 80% of total variance). Through this analysis and assessment of the 08–09 May time-series, it was determined that the peak of the 2013 population was best estimated from the mean of profiles collected between 06:30 h and 08:30 h, 09 May (2.3×10^{14}, $N = 8$, SE $= 2 \times 10^{13}$). Averaging effectively controlled for error associated with patchiness, such that most uncertainty in the final estimate of total cells was attributable to uncertainty in linear regression parameters ($\hat{\beta}_0$ and $\hat{\beta}_1$; 63% of total variance). Applying the same calculation to all profiles collected during the daytime IFCB profiling study on 13 May, the estimated total number of cells in the pond fell by 95% to 1.3×10^{13} ($N = 24$, SE $= 0.9 \times 10^{11}$).

Estimates of total cysts, new cyst recruitment, and cyst yield

The pre-bloom (November 2012) and post-bloom surveys of cyst abundance (July and November 2013) revealed common features in the cyst distribution across Salt Pond, in particular three prominent accumulation zones near the exit channel mouth and along the southwestern and northern shores (Fig. 9). The region near the mouth of the exit channel was not sampled directly in 2013 but has been confirmed as a region of elevated cyst abundance in surveys after blooms in 2015 and 2016. Most cysts were recruited to areas that are shallower than the depths of the chlorophyll maxima during the bloom's late development and termination phases (Fig. 10). Integration of the July 2013 survey map produced an estimated recruitment of 1.3×10^{13} total new cysts (SE $= 0.28 \times 10^{13}$) that was divided roughly evenly between the surface 0–1 cm and subsurface 1–3 cm sediment layers. Combined with the fluorometer-based estimate of peak planktonic cell abundance, the estimate of new cyst production corresponds to a yield of 10.9% (SE = 2.6%).

Across all three surveys, cyst concentrations tended to be greater in the surface 0–1 cm layer of the pond's sediment. Thus, sediment mixing did not vertically homogenize cyst concentrations between bloom termination and the fall

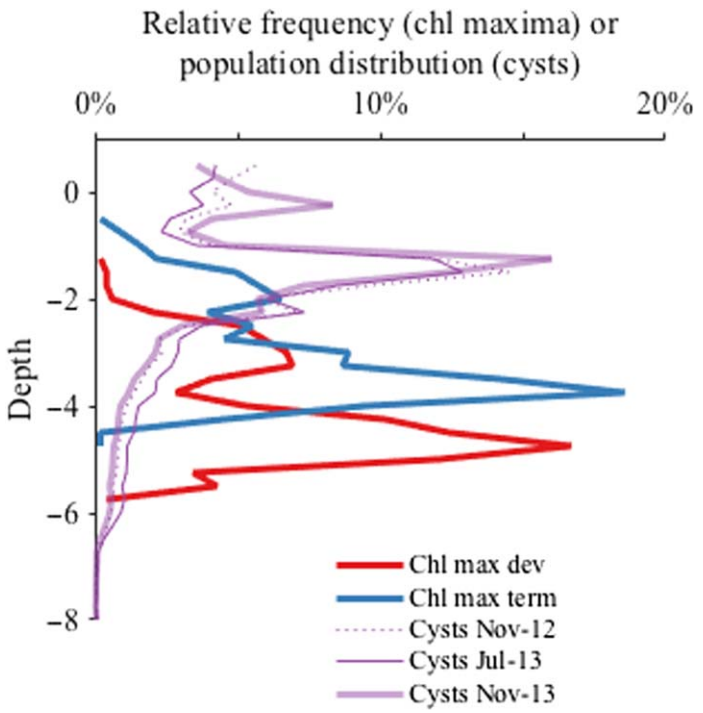

Fig. 10. Depths occupied by *A. catenella* planktonic and benthic stages derived from fluorescence profiles and spatial surveys of cyst abundance. Red and blue lines describe the relative frequency of chlorophyll maximum water depths (i.e., where planktonic stages were most concentrated) during the last 4 d of the bloom's development (05–09 May) and its termination phase (09–13 May), respectively. Purple lines describe the population distributions of cysts collected at corresponding bottom depths: one pre-bloom (November 2012) and two post-bloom (July and November 2013).

surveys (~ 6 months in 2013). When sampled about 2 months after bloom termination (July 2013), surface concentrations were ~ 2-fold greater than in the subsurface. Four months later surface concentrations were 44% greater than subsurface concentrations (November 2013), indicating an average rate of diffusive mixing of ~ 8 cm^2 yr^{-1}. In individual cores, surface layer concentrations were greater than the subsurface in 62% of the November 2012 cores, 77% of those collected in July 2013, and 74% of those collected November 2013.

Estimation of new cyst production relied on observations of the proportion of cysts having new morphology (p_{new}). The greatest p_{new} observed during the 2013 bloom was 88% (22 d from the bloom's gametogenic transition on 09 May), but these observations were limited to the surface 0–1 cm layer and at only a single location (the pond's northern shore). Subsequent sampling after the spring 2016 bloom showed that p_{new} is similar in surface and subsurface samples and across a wide area. The maximum p_{new} in 2016 was greater, reaching 97% and 95% of cysts in the 0–1 cm and 1–3 cm layers, respectively, 14 d after concerted gametogenesis. Cores collected the same day but at different locations within and immediately outside of Salt Pond were also similar or greater with respect to p_{new}. Informed by these results, the maximum p_{new} observed in 2013 (88%) was applied to all observations from both the 0–1 cm and 1–3 cm layers when estimating new cyst recruitment to Salt Pond.

Discussion

Through characterization of new cyst production by *A. catenella* in Salt Pond, several aspects of this species' behavior have been revealed for the first time. Among them are (1) much greater conversion of vegetative cells to zygotic resting cysts than has previously been documented in a natural bloom, (2) a life-cycle associated shift in vertical migration that may increase dispersal of cyst precursors (planozygotes; *see* Fig. 11), (3) predominance of encystment after planozygote settlement rather than in the water column, and (4) rapid infiltration of new cysts into subsurface sediments (here defined as >1 cm deep). Each of these findings has considerable implications for the ecology of *A. catenella* and likely many other meroplanktonic microbial eukaryotes whose long-term survival depends on sexual encystment and colonization (or recolonization) of favorable habitats.

This study also demonstrates for the first time, statistical methods for estimation of total cell and cyst population sizes that take advantage of the confined nature of Nauset blooms and newly developed sampling approaches, namely: automated observation of planktonic stages and counting of newly-formed cysts. Concerted sexual transitions by *A. catenella* blooms at the study site enables estimation of cyst yield, a measure of the robustness of new cyst production. Concerted gametogenesis and similar peak cell concentrations of Nauset blooms across multiple years (several million cells L^{-1}) suggests an association between sexual induction and exceedance of a cell density threshold. Each of these study outcomes is discussed in detail below.

Separation of bloom development and sexual induction in time

Cyst yield in studies of dinoflagellates and many other microbial eukaryotes is commonly understood to be the proportion of a dividing cell population that is transformed into new resting cysts. In culture experiments, dinoflagellate encystment is commonly induced through nutrient limitation (e.g., Anderson et al. 1984). In this context, vegetative cells divide until their internal stores of a limiting nutrient are exhausted, then form gametes and proceed toward encystment. Yield calculations often assume that all cells in a population proceed to successive stages of the life cycle at the same time, i.e., that production of new cells via vegetative division ceases at the onset of gametogenesis, sexual fusion and encystment. If instead, cell division and gametogenesis were to proceed in parallel, many more cysts than the peak number of planktonic cells might be produced,

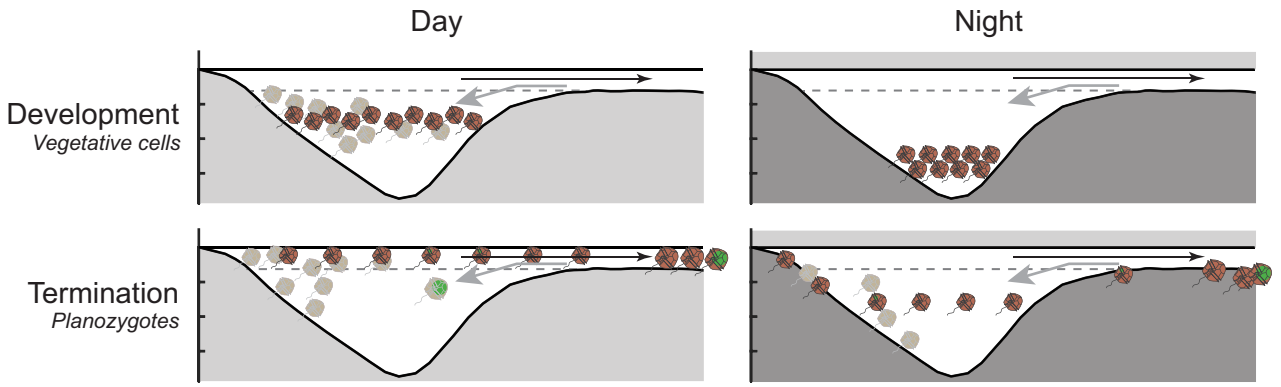

Fig. 11. Conceptual model of the interaction between life-cycle stage specific migration behaviors and tidal circulation during bloom development and termination. Day and nighttime *A. catenella* distributions (left and right columns) of vegetative and planozygote cells (top and bottom rows) are illustrated along the same bathymetry section as in Fig. 1. Long, weak ebb currents that evacuate surface water and short intense floods that displace water near the pond's exit channel mouth are denoted by black and gray vectors, respectively. Disruption of cell positions by floods is illustrated by grayed cells. Daytime surface avoidance by dividing vegetative cells promotes strong retention within the pond and accumulation. In contrast, daytime surface localization by planozygotes promotes export to the central marsh during ebbs and rapid bloom decline. Exported planozygotes as well as infections by the parasite *Amoebophrya* (indicated by green marks) continue to develop in the central marsh where they are also diluted. Some of these diluted and matured cells are reintroduced to the pond during floods (lower left, Fig. 6). Relatively shallow downward migrations at night lead to planozygote settlement and encystment around the pond's shallow periphery and exit channel as well as within the central marsh (lower right).

undermining the soundness of yield as a measure of encystment vigor (Olli and Anderson 2002).

Unlike batch laboratory cultures, *A. catenella* in Nauset can exploit environmental gradients in nutrient supply and remineralization that intensifies with spring warming (Anderson and Stolzenbach 1985). Nauset blooms therefore may be seldom, if ever, nutrient limited. It is unsurprising then that cysts are produced in the presence of relatively high nutrient concentrations (Anderson et al. 1983; Ralston et al. 2014; Brosnahan et al. 2015; and data presented here). Cyst yield remains a valid metric to describe the robustness of sexual transformation because, like nutrient starved cultures, the blooms undergo life-cycle transitions en masse (Figs. 4, 5; Brosnahan et al. 2015).

While sexual stages were observed prior to the bloom's peak on 09 May in 2013, there was a clear and concerted gametogenic transition during the 08–09 May overnight profiling study that also marked the onset of bloom decline (Figs. 4, 5). The $\sim$ 20% of the population that was not converted to gametes during this period was a mixture of vegetative cells and planozygotes, the latter having been formed from gamete fusions during days leading up to the bloom's peak. If this non-gamete portion were entirely planozygotes, the yield is more accurately estimated from the total number of haploid nuclei present, a counting approach that adds planozygote abundance again to the peak cell abundance (Anderson and Lindquist 1985). However, doing so only reduces our final yield estimate by $\sim$ 2%.

These observations naturally raise the question of what factor if not nutrient limitation triggers concerted gametogenesis. Across several years of IFCB deployments, sexual transitions in Salt Pond consistently occur when maximum cell concentrations exceed a few million cells L^{-1} (e.g., Brosnahan et al. 2015; data presented here and unpublished). These sexual transitions mark the end of bloom development and the onset of rapid decline, a pattern that commonly occurs in the southern Nauset blooms as well. Ralston et al. (2014) showed that interannual variability in the timing and magnitude of bloom peaks across all of the Nauset populations collapses when scaled using growing degree days; i.e., all bloom peaks occur at approximately the same growing degree day number. In effect, growing degree days are a proxy for total cell accumulation up to the threshold associated with sexual induction. Once this threshold is reached, cells cease division and populations decline rapidly.

Still, high cell density by itself is not sufficient to trigger gametogenesis. When cultured in nutrient replete medium, *A. catenella* frequently reaches concentrations greater than 10 million cells L^{-1} but seldom produces cysts (e.g., Anderson et al. 1984). Therefore, the trigger(s) may be one or more factors that are associated with these densities in natural settings. One such factor may be parasites like *Amoebophrya* whose spread is limited at lower host densities early in development (Chambouvet et al. 2008). Intensive investigation of *Amoebophrya* infections through the course of the 2012 Salt Pond bloom documented rapid spread of infections just as *A. catenella* undertook concerted gametogenesis, but found that mortality due to these infections accounted for $< 1\%$ of the bloom's overall decline (Velo-Suárez et al. 2013; Brosnahan et al. 2015). This coincidence in time between *A. catenella* sexual induction and onset of rapid infection suggests that the parasite plays a role in spurring its host's sexual induction.

Sexual induction of its host might be advantageous to the parasite as a means to increase the availability of suitable, long-lived habitats for survival through interbloom periods.

It has been shown that *Amoebophrya* infections of the dinoflagellate *Scrippsiella trochoidea* are passed to that host's cysts (Chambouvet et al. 2011), and we have similarly detected *Amoebophrya* ribosomal sequences in *A. catenella* cysts by polymerase chain reaction (PCR) (Sehein and Brosnahan unpubl.). Thus, the parasite appears to use its host's cysts as a refugium between blooms. The observed association between late stage infections and mature planozygotes further suggests that the parasite specifically targets diploid *A. catenella* stages (Fig. 6). Alternatively, the course of parasite infections may be altered with changes in host density and/or its sexual transitions, making infections of diploid hosts more readily observed. Such a host cue response has been shown in the flagellate *Parvilucifera sinerae*, another parasite that is stimulated by elevated levels of dimethylsulphide, a compound produced by its dinoflagellate hosts notably including *Alexandrium* (Garcés et al. 2013). Such interactions reflect so-called Red Queen type antagonistic coevolution through which, for instance, concerted gametogenesis by *A. catenella* may have evolved as a means to escape from *Amoebophrya* and, in response, *Amoebophrya* has evolved the ability to recognize and exploit its host's life cycle transitions.

Other environmental and ecological factors may induce sexuality instead of or in addition to ones involving parasitic attack. Another example of a highly induced *A. catenella* population was recorded in the Gulf of Maine in 2009. During that event, cells reached similar peak concentrations but lacked parasite infections (Brosnahan et al. 2014; McGillicuddy et al. 2014). Were concerted gametogenesis to have evolved as a defense against infection, the proximate trigger need not be a produced by a parasite. Instead, *A. catenella* might produce its own autocrine trigger whose production is linked to a combination of cell density, stress, and other stimuli that reliably anticipate the spread of infections in those habitats where parasites are present.

Encystment occurs after planozygote settlement

The appearance of new resting cysts lagged the disappearance of planktonic stages by more than a week, yet this is the approximate lifetime of the planozygote stage in culture experiments (Anderson and Lindquist 1985; Figueroa et al. 2005). The culture-derived result suggests that, following a complete conversion to gametes, a bloom would fall to and remain at a near half-fold density for up to a week while planozygotes complete their maturation and encyst. Instead, the planktonic population in Salt Pond fell by 75–95% within just 4 d of its peak and without substantial accumulation of new cysts in the pond's sediment (09 and 13 May; Fig. 4). Nine days later (22 May), after a period during which *A. catenella* was all but absent from the water column, new cysts began to accumulate, new cyst fractions (p_{new}) increased from 0% to 84%, and cyst capture by tube traps increased dramatically. An additional 9 d later—a period through which planktonic *A. catenella* abundance remained near 0—cyst numbers increased another 2.5-fold and p_{new} increased to 88%.

Immediately after their formation, *A. catenella* planozygotes are similar in size to vegetative cells, making these two life stages difficult to distinguish on a cell-by-cell basis. As planozygotes mature, they grow larger, eventually exceeding the size of the largest vegetative cells (Anderson et al. 1983; Brosnahan et al. 2015). Such large cells were observed throughout the late development and termination periods but did not represent a meaningful fraction of the population until after 13 May when most of the population had already dissipated without significant new cyst production (Figs. 4, 5). By 22 May, planktonic cells were all but undetected, yet 70% of new cysts had not yet been formed (Fig. 4). If the remaining planktonic cells were the source of the last-appearing cysts, average concentrations would have needed to be $> 30{,}000$ cells L^{-1}. Instead, the maximum concentration observed over this final observation period was just 8 cells L^{-1}.

It is also highly unlikely that the bulk of cysts ultimately recruited to the pond could have been formed outside it then advected back in during floods. Though detected, cysts were quite rare in the IFCB image record. Further any cysts advected back into the pond would have settled rapidly in its slow moving currents. Given these dynamics, a larger proportion of cysts would be expected to settle within the deep central hole than was observed (Fig. 9).

A more cogent explanation for the bloom's rapid dissipation is that planozygotes settled on the bottom before encystment. While planozygotes were not observed directly in sediment samples collected through this study, the processing of these samples included vigorous disaggregation with a sonicating probe, a treatment that destroys any planozygotes or other planktonic stages present. Over several years colleagues have noted red pigmentation of sediments at the north shore accumulation area within Salt Pond in the days following bloom peaks. Similarly, after blooms in another part of Nauset in 2012 and 2013, installed sampling equipment was covered by sticky mats of planozygotes. Though not quantitative, these observations also indicate settlement of planozygotes prior to cyst formation.

Our observation in 2016 that new cysts appeared in similar proportions in the surface and subsurface sediment samples just 2 weeks after gametogenesis highlights one consequence of pre-encystment settlement, namely that planozygotes will infiltrate sediments before encysting. We speculate two possible mechanisms that could deliver new cysts to subsurface sediments. The first is simple passive mixing, either through physical sediment disturbance or bioturbation. If most planozygotes were formed by 12 May in 2013, their maturation period was 10–19 d, substantially longer than observed in culture ($\sim$ 7 d; Anderson and Lindquist 1985; Figueroa et al. 2005). Past characterization of *A. catenella* cyst burial in a similar coastal pond calculated a

diffusive mixing rate of 20 cm^2 yr^{-1} from observed Pb-210 and Th-234 profiles (Keafer et al. 1992). This is faster than was estimated from changes in the mean surface and subsurface cyst concentrations after the 2013 bloom ($\sim$ 8 cm^2 yr^{-1}), but more reasonable for mixing immediately after the bloom and before onset of summertime anoxia. Applying the greater of these mixing rates, up to 17% of planozygotes might have been dispersed into the 1–3 cm sediment layer 2 weeks after their formation. The resulting new cysts would then have been comparable in abundance to old ones in the subsurface (i.e., $p_{new} \sim 50\%$), but this is not what was observed in 2016. Instead, p_{new} was highly enriched in both the surface and subsurface layers (97% and 95%, respectively).

A second explanation for the appearance of cysts in subsurface sediments is that planozygotes might actively swim into sediment interstices. Exactly this behavior has been observed in cultures of the dinoflagellate *Karenia brevis* (Sinclair and Kamykowski 2008). Similarity in the recruitment pattern between years (2012, 2013 as well as after subsequent blooms in 2015 and 2016) may reflect habitat selectivity on the part of planozygotes (Fig. 9), e.g., planozygotes might seek specific chemical cues or gradients when settling. Figueroa et al. (2005) showed that *Alexandrium* encystment was more robust when planozygotes were transferred from nutrient-limited to replete medium. Perhaps the extended lifetime of planozygotes in situ reflects time needed to reach subsurface sediments that are ideal for encystment. It may also be that encystment within subsurface anoxic zones beneficially suppresses germination (Anderson et al. 1987) or grazing by benthic animals (e.g., Steyaert et al. 2007).

Direct estimation of total cells, new cyst production, and cyst yield by a natural bloom

Accurate quantification of new cyst production in a complex natural system requires combined observational and statistical approaches that estimate the abundance of relevant life cycle stages, characterize estimate uncertainties, and provide adequate temporal resolution to resolve relationships between precursor stages and cysts. These challenges were addressed here through a combination of high-frequency, automated observation of the relatively fast-changing, planktonic fraction of a population and intensive, manual sampling of its slower-changing resting cyst fraction. In turn, estimates of abundance and their uncertainty were developed using statistical approaches that account for contributions from spatial patterns, patchiness, and uncertainty in the relationship between *A. catenella* biovolume and fluorescence.

Confidence in population size estimates from a single profiling fluorometer is grounded in the exceptional degree of past characterization of *A. catenella* blooms in Salt Pond. Near bloom peaks *A. catenella* is often numerically dominant among the microplankton present (Brosnahan et al. 2015). This species is also chlorophyll rich on a per cell basis (MacIntyre et al. 1997). In situ calibration of the fluorescence profiles with IFCB observations enabled direct assessment of fluorescence $cell^{-1}$, which in many phytoplankton communities varies in response to a wide variety of factors including exposure to near-surface irradiance, diel cycling, and nutrient limitation (Falkowski and Kiefer 1985). The lack of such variability here may be attributable to vertical migrations by this species, which likely limit both nutrient limitation and photoinhibition (Fig. 8; Anderson and Stolzenbach 1985).

Individual estimates of the planktonic population size through the course of the overnight profiling study were remarkably consistent at $\sim 1 \times 10^{14}$ cells until the pre-dawn period when phased division and vertical migration coincided with an increase to 2.3×10^{14} cells (Fig. 8). While the timing of this increase was expected, its magnitude is puzzling given the population's life cycle stage composition. Prior to division, $\sim$ 40% were gametes with the remainder some combination of vegetative cells and early-stage planozygotes (Fig. 5). After division, approximately 20% remained as non-gamete cells. Assuming the larger, post-division cells were early stage planozygotes, only $\sim$ 15% of the pre-division population would have contributed to the observed cell increase, requiring these cells to undergo more than three divisions. We suggest two mechanisms to explain this observation: (1) multi-division gametogenesis and (2) bottom localization by some portion of the population until the morning ascent.

Gametogenesis has previously been associated with a surge in division through cultures studies that used phosphate stress for sexual induction (Anderson and Lindquist 1985). In Salt Pond, quadruplets and triplets of gamete-sized cells (formed through rapid, successive divisions) were most frequently observed during the afternoon and evening of the overnight profiling study, occasionally reaching frequencies of 1–2%. However, frequency estimates were based on five or fewer such chains per IFCB sample, leading to large sample-to-sample uncertainties. Binning the IFCB observations by day produced the same pattern, but differences in chain frequencies were still not statistically significant between development and gametogenic periods.

The second mechanism, that the especially large increase in total cells resulted from vertical migration from the pond's bottom, is suggested by the lower limit of these cells' ambit and the pond's bottom depth distribution. For a population evenly distributed at 2–3 m depth during daytime, about half of the downward swimming cells would encounter the bottom before reaching their deeper migration limit ($\sim$ 5 m; Figs. 1, 8, and 11). Such cells might aggregate at the water-sediment interface or enter the sediment where they could absorb concentrated nutrients much like cells in deeper regions of the pond.

Discrepancies between bottle and fluorometer based estimates of the total number of planktonic cells are most likely

due to under-sampling with bottles. The 2-m spacing between these samples was ill-suited for capturing the most concentrated layers observed during daytime ebbs and overnight periods when more than half of total integrated fluorescence was present within 0.5 m of the chlorophyll maximum. For this reason, the fluorometer-based estimates were used to calculate cyst yield. Use of bottle-based total cell estimates increases yield estimates more than twofold.

The reported 10.9% yield is further conservative because it neglects substantial numbers of cysts. Spatial surveys in 2013 did not investigate deposition within the exit channel or nearby Salt Pond Bay, areas where new cyst concentrations were comparable to those within the pond after the 2016 bloom. Neighboring Salt Pond Bay has about seven times the area of Salt Pond (Fig. 1), so, if cyst concentrations were similar across all three areas (the pond, channel and Salt Pond Bay) as much as 80% of the peak cell population might have been converted into new cysts in 2013. For comparison, sediment trap-based approaches have produced yield estimates between 1% and 2% (Garcès et al. 2004; Anglès et al. 2012; Cosgrove et al. 2014), > 5-fold lower than even our pond-only estimate.

Robust conversion of vegetative cells to new planozygotes

Measurement of cyst yield also constrains the role of other loss processes in bloom termination. Concerted gametogenesis by Salt Pond blooms presents a natural experiment whereby further cell proliferation is blocked at the bloom's peak. Blooms then dissipate through a combination of encystment, dilution, grazing, parasitism, cell death, and other forms of mortality. Unlike other processes, losses to encystment can be verified directly through post-bloom benthic surveys. Encystment is also a multi-step process that poses a series of barriers to cyst formation (i.e., gametogenesis, gamete fusion, and encystment), each of which can be examined through analysis of IFCB images to determine the timing and relative importance of these potential bottlenecks to encystment vs. other co-occurring loss mechanisms.

Overall, progression toward encystment appears to have been quite robust. In past IFCB-based studies and in the record collected here, gamete-gamete fusions were exclusively composed of small cells that spiked in abundance at the bloom's peak (Fig. 5; Brosnahan et al. 2015). All small singlet cells (estimated volume < 14,260 μm^3) were designated as gametes and made up ~ 80% of the peak population. The remaining 20% was again some combination of vegetative cells and new planozygotes since both gamete-sized cells and gamete-gamete fusions were recorded prior to the bloom's peak. Thus, gametogenesis, the first step in the encystment pathway, was both concerted and nearly complete in its extent.

The next step toward encystment is gamete-gamete pairing. Though the *A. catenella* mating system is complex, pairing is most likely mediated through a simple binary adhesion system (Brosnahan et al. 2010). Given the high cell densities observed during the bloom's gametic period, gamete encounter likely presented a minimal barrier to planozygote formation. The fusion time for *A. catenella* gametes (t_{fus}) inferred from the vertical distribution of fusing cells is similar to those observed directly in other dinoflagellates (~ 1 h; Stosch 1973; Coats et al. 1984; Figueroa and Bravo 2005). Calculations from gamete fusion frequencies demonstrate the inverse relationship between t_{fus} and F_{fus}, the proportion of the population estimated to complete fusion (Fig. 7). It is revealing that at 100% pairing success ($F_{fus} = 1$, corresponding to the minimum of t_{fus}), t_{fus} calculated in this way is 2 h, twice the value estimated from their distribution.

One reason the frequency-based calculation may have produced a long t_{fus} estimate is that this quantity represents the total time that cells spend fusing. In other *Alexandrium* species, cells may undergo multiple rounds of fusion and division prior to (or instead of) encysting (Figueroa et al. 2006; Figueroa et al. 2015). Similar behavior by *A. catenella* would cause frequency-based estimates of t_{fus} to be long because a single cell might undergo multiple rounds of fusion, division back to its haploid form, and re-fusion. Though observed oscillations in mean cell size 09–12 May superficially appear to support such a model (Fig. 5), the lack of a diel pattern in the abundance of fusing gametes (Fig. 8) and the association of daytime cell size increases with tide floods (Figs. 6, 11) favor an alternative explanation: that new planozygotes were being removed from the planktonic population at higher rates than other stages. Observed frequencies of gamete fusion were therefore increasingly inflated through time as more and more planozygotes either settled on the bottom or were exported from the pond.

Precise estimation of the proportion of gametes completing fusion therefore must consider planozygote removal. One way to minimize this effect is to consider shorter intervals when most planozygotes either had not yet formed or been removed. Doing so, and assuming that $t_{fus} = 1$ h, suggests that as much as two thirds of the gamete population fused within 5 h of the bloom's peak, again indicating robust progression toward encystment and comparatively small losses due to other processes.

Daytime surface localization by planozygotes directs cyst dispersal

Vertical migration by *A. catenella* and other dinoflagellates has long been interpreted as a means to exploit opposing gradients of light and nutrients within the water column (Anderson and Stolzenbach 1985; MacIntyre et al. 1997). Consistent with this interpretation, Salt Pond *A. catenella* ascend to a fixed daytime light intensity during bloom development (30–40% of maximum surface irradiance; data not shown). This pattern changes, however, in the days following gametogenic events when surface waters are discolored red during the day, indicative of concentrations > 500,000 cells L^{-1}. Such red

water events typically last for just the first 2 d after gametogenesis and have never been observed in the days leading up to these transitions when overall cell abundance is similar (observed in 2012, 2013, 2015, and 2016). Comparable planozygote enrichment and surface red water was also observed in the 2009 Gulf of Maine event (McGillicuddy et al. 2014). In Nauset, these surface enrichments have been observed under conditions ranging from full sunlight to overcast. Clearly then *A. catenella* planozygotes abandon the light "ceiling" observed by vegetative populations and instead aggregate at the physical barrier imposed by the surface (Figs. 8, 11).

An important consequence of this behavioral shift is that the dispersal of planozygotes (and new resting cysts) is altered from that experienced by their vegetative progenitors. Within Nauset, near surface swimming promotes heightened export from the kettle ponds, expanding the area affected by *A. catenella* and its toxins (Fig. 11). A hydrodynamic modeling study found that such surface seeking behavior reduced the residence time of cells within Salt Pond by as much as half relative to the surface avoidance behavior exhibited by vegetative cells (Ralston et al. 2015). This corresponds with cyst deposition in the pond's exit channel and export to the far reaches of Salt Pond Bay. It is likely that the same occurs in other areas, promoting leakage from inshore features that would otherwise retain blooms and promote their intensification. Planozygote swimming behavior (and associated enhancement of dispersal) likely promotes the colonization of new habitats and establishment of genetic connectivity between neighboring populations. Indeed, a previous microsatellite-based study did not find genetic differences between populations centered in the respective Nauset ponds, even though they exhibit independent dynamics and appear to experience very limited exchange (Richlen et al. 2012).

Near-surface localization is also likely to direct dispersal of planozygotes formed within open coastal blooms. *A. catenella* and many other dinoflagellates favor conditions of increasing water stratification and reduced storm-driven mixing (Margalef 1978; Smayda 1997), precisely the conditions that are correlated with enhanced surface transport by land and sea breezes. In studies of other near surface localized organisms (neuston), Tapia et al. (2004) demonstrated shoreward transport of as much as 2 km d^{-1} due to sea breezes in northern Baja California. Similarly, a modeling study of larval lobster dispersal within the Gulf of Maine found strong shoreward transport of animals when forced by modest sea breezes (Incze and Naimie 2000).

In Salt Pond, surface localization appears to occur only during daytime; fluorescence maxima continued to migrate downward overnight though to shallower and shallower limits (Fig. 8). If coastal bloom planozygotes were to behave similarly, downward migrations at night might limit seaward transport caused by land breezes. While land and sea breezes are known to weaken with distance from shore, *A. catenella* blooms within 10–20 km of coasts likely experience this alternating forcing. Exploitation of sea breezes and other air–sea interactions may promote cyst settlement in shallower waters where return to the euphotic zone by germlings is made easier (Vahtera et al. 2014). Shoreward transport of offshore populations may also promote colonization of new inshore habitats like Nauset.

Conclusion

Through this study, which was initiated with the narrow aim of determining the production rate of new cysts by a natural *A. catenella* bloom, several aspects of this organism's life history have been revealed for the first time. Among these are daytime surface localization by planozygotes, heightened susceptibility of planozygotes to the parasite *Amoebophrya*, infiltration of planozygotes into bottom sediment prior to encystment, and robust conversion of planktonic cells to new resting cysts. These outcomes underscore the importance of resting cysts for the survival and spread of this species and others, like *Amoebophrya*, that are dependent on its blooms. New observing and analytical methods for estimation of total population sizes facilitated these discoveries and point to a need to more carefully observe and consider bottom interactions by otherwise free-living life cycle stages. It also remains to be shown to what extent these behaviors are exhibited in larger coastal blooms that deposit cysts in deeper waters (e.g., 100–200 m deep; Anderson et al. 2014). Do planozygotes actively swim to the bottom after a finite dispersal period? Do they similarly infiltrate sediment and to what extent is sediment infiltration an active process? To what extent (if any) is new cyst recruitment mediated by habitat selectivity on the part of these cells? Many of these questions are directly analogous to those considered in dispersal studies of larger, larval animals. Addressing them in the context of *A. catenella*, a single celled organism that negatively impacts ecosystems and public health through its production of PSP neurotoxins, has wide-ranging implications for studies of natural selection by coastal ocean habitats and the biogeography of this and other cyst-forming plankton species.

References

Anderson, D. 1997. Bloom dynamics of toxic *Alexandrium* species in the northeastern US. Limnol. Oceanogr. **42**: 1009–1022. doi:10.4319/lo.1997.42.5_part_2.1009

Anderson, D., D. Kulis, and B. Binder. 1984. Sexuality and cyst formation in the dinoflagellate *Gonyaulax tamarensis*: Cyst yield in batch cultures. J. Phycol. **20**: 418–425. doi: 10.1111/j.0022-3646.1984.00418.x

Anderson, D., and N. Lindquist. 1985. Time-course measurements of phosphorus depletion and cyst formation in the dinoflagellate *Gonyaulax tamarensis* Lebour. J. Exp. Mar. Biol. Ecol. **86**: 1–13. doi:10.1016/0022-0981(85)90039-5

Anderson, D., and K. Stolzenbach. 1985. Selective retention of two dinoflagellates in a well-mixed estuarine embayment: The importance of diel vertical migration and surface avoidance. Mar. Ecol. Prog. Ser. **25**: 39–50. doi:10.3354/meps025039

Anderson, D., C. Taylor, and E. Armbrust. 1987. The effects of darkness and anaerobiosis on dinoflagellate cyst germination. Limnol. Oceanogr. **32**: 340–351. doi:10.4319/lo.1987.32.2.0340

Anderson, D. M. 1980. Effects of temperature conditioning on development and germination of *Gonyaulax tamarensis* (Dinophyceae) hypnozygotes. J. Phycol. **16**: 166–175. doi:10.1111/j.1529-8817.1980.tb03013.x

Anderson, D. M., S. W. Chisholm, and C. J. Watras. 1983. Importance of life cycle events in the population dynamics of *Gonyaulax tamarensis*. Mar. Biol. **76**: 179–189. doi:10.1007/BF00392734

Anderson, D. M., Y. Fukuyo, and K. Matsuoka. 2003. Cyst methodologies, p. 165–190. *In* G. M. Hallegraeff, D. M. Anderson, and A. D. Cembella [eds.], Manual on harmful marine microalgae, Monographs on oceanographic methodology, V. 11.

Anderson, D. M., D. M. Kulis, B. A. Keafer, K. E. Gribble, R. Marin, and C. A. Scholin. 2005. Identification and enumeration of *Alexandrium* spp. from the Gulf of Maine using molecular probes. Deep-Sea Res. Part II Top. Stud. Oceanogr. **52**: 2467–2490. doi:10.1016/j.dsr2.2005.06.015

Anderson, D. M., T. J. Alpermann, A. D. Cembella, Y. Collos, E. Masseret, and M. Montresor. 2012. The globally distributed genus *Alexandrium*: Multifaceted roles in marine ecosystems and impacts on human health. Harmful Algae **14**: 10–35. doi:10.1016/j.hal.2011.10.012

Anderson, D. M., and others. 2014. *Alexandrium catenella* cysts in the Gulf of Maine: Long-term time series of abundance and distribution, and linkages to past and future blooms. Deep-Sea Res. Part II Top. Stud. Oceanogr. **103**: 6–26. doi:10.1016/j.dsr2.2013.10.002

Anglès, S., E. Garcés, T. K. Hattenrath-Lehmann, and C. J. Gobler. 2012. In situ life-cycle stages of *Alexandrium catenella* during bloom development in Northport Harbor (New York, USA). Harmful Algae **16**: 20–26. doi:10.1016/j.hal.2011.12.008

Aubrey, D. G., and P. E. Speer. 1985. A study of non-linear tidal propagation in shallow inlet/estuarine systems part I: Observations. Estuarine **21**: 185–205. doi:10.1016/0272-7714(85)90096-4

Brosnahan, M. L., D. M. Kulis, A. R. Solow, D. L. Erdner, L. Percy, J. Lewis, and D. M. Anderson. 2010. Outbreeding lethality between toxic Group I and nontoxic Group III *Alexandrium tamarense* spp. isolates: Predominance of heterotypic encystment and implications for mating interactions and biogeography. Deep-Sea Res. Part II Top. Stud. Oceanogr. **57**: 175–189. doi:10.1016/j.dsr2.2009.09.005

Brosnahan, M. L., S. Farzan, B. A. Keafer, H. M. Sosik, R. J. Olson, and D. M. Anderson. 2014. Complexities of bloom dynamics in the toxic dinoflagellate *Alexandrium catenella* revealed through DNA measurements by imaging flow cytometry coupled with species-specific rRNA probes. Deep-Sea Res. Part II Top. Stud. Oceanogr. **103**: 185–198. doi:10.1016/j.dsr2.2013.05.034

Brosnahan, M. L., and others. 2015. Rapid growth and concerted sexual transitions by a bloom of the harmful dinoflagellate *Alexandrium catenella* (Dinophyceae). Limnol. Oceanogr. **60**: 2059–2078. doi:10.1002/lno.10155

Chambouvet, A., P. Morin, D. Marie, and L. Guillou. 2008. Control of toxic marine dinoflagellate blooms by serial parasitic killers. Science **322**: 1254–1257. doi:10.1126/science.1164387

Chambouvet, A., C. Alves-de-Souza, V. Cueff, D. Marie, S. Karpov, and L. Guillou. 2011. Interplay between the parasite *Amoebophrya* sp.(Alveolata) and the cyst formation of the red tide dinoflagellate *Scrippsiella trochoidea*. Protist **162**: 637–649. doi:10.1016/j.protis.2010.12.001

Chisholm, S. W., and R. E. McDuff. 1982. The calculation of in situ growth rates of phytoplankton populations from fractions of cells undergoing mitosis: A clarification. Limnol. Oceanogr. **27**: 783–788. doi:10.4319/lo.1982.27.4.0783

Choi, C. J., M. L. Brosnahan, T. R. Sehein, D. M. Anderson, and D. L. Erdner. 2017. Insights into the loss factors of phytoplankton blooms: The role of cell mortality in the decline of two inshore Alexandrium blooms. Limnol. Oceanogr. **62**: 1742–1753. doi:10.1002/lno.10530

Coats, D. W., M. A. Tyler, and D. M. Anderson. 1984. Sexual processes in the life cycle of *Gyrodinium uncatenum* (Dinophyceae): A morphogenetic overview. J. Phycol. **20**: 351–361. doi:10.1111/j.0022-3646.1984.00351.x

Cosgrove, S., A. N. Rathaille, and R. Raine. 2014. The influence of bloom intensity on the encystment rate and persistence of *Alexandrium minutum* in Cork Harbor, Ireland. Harmful Algae **31**: 114–124. doi:10.1016/j.hal.2013.10.015

Crespo, B. G., B. A. Keafer, D. K. Ralston, H. Lind, D. Farber, and D. M. Anderson. 2011. Dynamics of *Alexandrium catenella* blooms and shellfish toxicity in the Nauset Marsh System of Cape Cod (Massachusetts, USA). Harmful Algae **12**: 26–38. doi:10.1016/j.hal.2011.08.009

Falkowski, P., and D. A. Kiefer. 1985. Chlorophyll a fluorescence in phytoplankton: Relationship to photosynthesis and biomass. J. Plankton Res. **7**: 715–731. doi:10.1093/plankt/7.5.715

Figueroa, R., and I. Bravo. 2005. Sexual reproduction and two different encystment strategies of *Lingulodinium polyedrum* (Dinophyceae). J. Phycol. **41**: 370–379. doi:10.1111/j.1529-8817.2005.04150.x

Figueroa, R., I. Bravo, and E. Garcés. 2005. Effects of nutritional factors and different parental crosses on the

encystment and excystment of *Alexandrium catenella* (Dinophyceae) in culture. Phycologia **44**: 658–670. doi:10.2216/0031-8884(2005)44[658:EONFAD]2.0.CO;2

Figueroa, R. I., I. Bravo, and E. Garcés. 2006. Multiple routes of sexuality in *Alexandrium taylori* (Dinophyceae) in culture. J. Phycol. **42**: 1028–1039. doi:10.1111/j.1529-8817.2006.00262.x

Figueroa, R. I., J. A. Vázquez, A. Massanet, M. A. Murado, and I. Bravo. 2011. Interactive effects of salinity and temperature on planozygote and cyst formation of *Alexandrium minutum* (Dinophyceae) in culture. J. Phycol. **47**: 13–24. doi:10.1111/j.1529-8817.2010.00937.x

Figueroa, R. I., C. Dapena, I. Bravo, and A. Cuadrado. 2015. The hidden sexuality of *Alexandrium minutum*: An example of overlooked sex in dinoflagellates. PLoS One **10**: e0142667. doi:10.1371/journal.pone.0142667

Fraga, S., N. Sampedro, J. Larsen, Ø. Moestrup, and A. J. Calado. 2015. Arguments against the proposal 2302 by John & al. to reject the name *Gonyaulax catenella* (*Alexandrium catenella*). Taxon **64**: 634–635. doi:10.12705/643.15

Garcés, E., I. Bravo, M. Vila, R. I. Figueroa, M. Masó, and N. Sampedro. 2004. Relationship between vegetative cells and cyst production during *Alexandrium minutum* bloom in Arenys de Mar harbour (NW Mediterranean). J. Plankton Res. **26**: 637–645. doi:10.1093/plankt/fbh065

Garcés, E., E. Alacid, A. Reñé, K. Petrou, and R. Simo. 2013. Host-released dimethylsulphide activates the dinoflagellate parasitoid *Parvilucifera sinerae*. ISME J. **7**: 1065. doi:10.1038/ismej.2012.173

Hastie, T. J., and R. J. Tibshirani. 1990. Generalized additive models. V. **43**. CRC Press.

Incze, L. S., and C. E. Naimie. 2000. Modelling the transport of lobster (*Homarus americanus*) larvae and postlarvae in the Gulf of Maine. Fish. Oceanogr. **9**: 99–113. doi:10.1046/j.1365-2419.2000.00125.x

John, U., R. W. Litaker, M. Montresor, S. Murray, M. L. Brosnahan, and D. M. Anderson. 2014*a*. Formal revision of the *Alexandrium tamarense* species complex (Dinophyceae): The introduction of five species with emphasis on molecular-based (rDNA) classification. Protist **165**: 779–804. doi:10.1016/j.protis.2014.10.001

John, U., W. Litaker, M. Montresor, S. Murray, M. L. Brosnahan, and D. M. Anderson. 2014*b*. (2302) Proposal to reject the name *Gonyaulax catenella* (*Alexandrium catenella*) (Dinophyceae). Taxon **63**: 932–933. doi:10.12705/634.21

Keafer, B. A., K. O. Buesseler, and D. M. Anderson. 1992. Burial of living dinoflagellate cysts in estuarine and nearshore sediments. Mar. Micropaleontol. **20**: 147–161. doi:10.1016/0377-8398(92)90004-4

Kokinos, J. P., and D. M. Anderson. 1995. Morphological development of resting cysts in cultures of the marine dinoflagellate *Lingulodinium polyedrum* (= *L. machaerophorum*). Palynology **19**: 143–166. doi:10.1080/01916122.1995.9989457

Lilly, E. L., K. M. Halanych, and D. M. Anderson. 2007. Species boundaries and global biogeography of the *Alexandrium tamarense* complex (Dinophyceae). J. Phycol. **43**: 1329–1338. doi:10.1111/j.1529-8817.2007.00420.x

MacIntyre, J., J. Cullen, and A. Cembella. 1997. Vertical migration, nutrition and toxicity in the dinoflagellate *Alexandrium tamarense*. Mar. Ecol. Prog. Ser. **148**: 201–216. doi:10.3354/meps148201

Margalef, R. 1978. Life-forms of phytoplankton as survival alternatives in an unstable environment. Oceanol. Acta **134**: 493–509.

Margulis, L., D. Sagan, and L. Olendzenski. 1985. What is sex?, p. 69–85. In H. O. Halverson, and A. Monroy [eds.], The Origin and Evolution of Sex, Alan R. Liss, New York.

McGillicuddy, Jr., D. J., and others. 2014. A red tide of *Alexandrium catenella* in the Gulf of Maine. Deep-Sea Res. Part II Top. Stud. Oceanogr. **103**: 174–184. doi:10.1016/j.dsr2.2013.05.011

Moberg, E. A., and H. M. Sosik. 2012. Distance maps to estimate cell volume from two-dimensional plankton images. Limnol. Oceanogr.: Methods **10**: 278–288. doi:10.4319/lom.2012.10.278

Nagai, S., Y. Matsuyama, S.-J. Oh, and S. Itakura. 2004. Effect of nutrients and temperature on encystment of the toxic dinoflagellate *Alexandrium tamarense* (Dinophyceae) isolated from Hiroshima Bay, Japan. Plankton Biol. Ecol. **51**: 103–109.

Olli, K., and D. Anderson. 2002. High encystment success of the dinoflagellate *Scrippsiella* cf. *lachrymosa* in culture experiments. J. Phycol. **38**: 145–156. doi:10.1046/j.1529-8817.2002.01113.x

Olson, R., and H. Sosik. 2007. A submersible imaging-in-flow instrument to analyze nano-and microplankton: Imaging FlowCytobot. Limnol. Oceanogr.: Methods **5**: 195–203. doi:10.4319/lom.2007.5.195

Prud'homme van Reine, W. F. 2017. Report of the nomenclature committee for algae: 15. Taxon **66**: 191–192. doi:10.12705/661.16

Ralston, D. K., B. A. Keafer, M. L. Brosnahan, and D. M. Anderson. 2014. Temperature dependence of an estuarine harmful algal bloom: Resolving interannual variability in bloom dynamics using a degree-day approach. Limnol. Oceanogr. **59**: 1112–1126. doi:10.4319/lo.2014.59.4.1112

Ralston, D. K., M. L. Brosnahan, S. E. Fox, K. D. Lee, and D. M. Anderson. 2015. Temperature and residence time controls on an estuarine harmful algal bloom: Modeling hydrodynamics and *Alexandrium catenella* in Nauset Estuary. Estuaries Coast. **38**: 2240–2258. doi:10.1007/s12237-015-9949-z

Richlen, M. L., D. L. Erdner, L. A. R. McCauley, K. Libera, and D. M. Anderson. 2012. Extensive genetic diversity and rapid population differentiation during blooms of *Alexandrium catenella* (Dinophyceae) in an isolated salt pond on Cape Cod, MA, USA. Ecol. Evol. **2**: 2588–2599. doi:10.1002/ece3.373

Rines, J. E. B., M. N. Mcfarland, P. L. Donaghay, and J. M. Sullivan. 2010. Thin layers and species-specific characterization of the phytoplankton community in Monterey Bay, California, USA. Cont. Shelf Res. **30**: 66–80. doi:10.1016/j.csr.2009.11.001

Schwinghamer, P., D. Anderson, and D. Kulis. 1991. Separation and concentration of living dinoflagellate resting cysts from marine sediments via density-gradient centrifugation. Limnol. Oceanogr. **36**: 588–592. doi:10.4319/lo.1991.36.3.0588

Sinclair, G. A., and D. Kamykowski. 2008. Benthic-pelagic coupling in sediment-associated populations of *Karenia brevis*. J. Plankton Res. **30**: 829–838. doi:10.1093/plankt/fbn042

Smayda, T. J. 1997. Harmful algal blooms: Their ecophysiology and general relevance to phytoplankton blooms in the sea. Limnol. Oceanogr. **42**: 1137–1153. doi:10.4319/lo.1997.42.5_part_2.1137

Sosik, H. M., and R. J. Olson. 2007. Automated taxonomic classification of phytoplankton sampled with imaging-in-flow cytometry. Limnol. Oceanogr.: Methods **5**: 204–216.

Steidinger, K. A. 2010. Research on the life cycles of harmful algae: A commentary. Deep-Sea Res. Part II Top. Stud. Oceanogr. **57**: 162–165. doi:10.1016/j.dsr2.2009.09.001

Steyaert, M., L. Moodley, T. Nadong, T. Moens, K. Soetaert, and M. Vincx. 2007. Responses of intertidal nematodes to short-term anoxic events. J. Exp. Mar. Biol. Ecol. **345**: 175–184. doi:10.1016/j.jembe.2007.03.001

Storlazzi, C. D., M. E. Field, and M. H. Bothner. 2010. The use (and misuse) of sediment traps in coral reef environments: Theory, observations, and suggested protocols. Coral Reefs **30**: 23–38. doi:10.1007/s00338-010-0705-3

Tapia, F. J., J. Pineda, F. J. Ocampo-Torres, H. L. Fuchs, P. E. Parnell, P. Montero, and S. Ramos. 2004. High-frequency observations of wind-forced onshore transport at a coastal site in Baja California. Cont. Shelf Res. **24**: 1573–1585. doi:10.1016/j.csr.2004.03.013

Vahtera, E., B. G. Crespo, D. J. McGillicuddy, K. Olli, and D. M. Anderson. 2014. *Alexandrium catenella* cyst viability and germling survival in light vs. dark at a constant low temperature. Deep-Sea Res. Part II Top. Stud. Oceanogr. **103**: 112–119. doi:10.1016/j.dsr2.2013.05.010

Velo-Suárez, L., M. L. Brosnahan, D. M. Anderson, and D. J. McGillicuddy. 2013. A quantitative assessment of the role of the parasite *Amoebophrya* in the termination of *Alexandrium catenella* blooms within a small coastal embayment. PLoS One **8**: e81150. doi:10.1371/journal.pone.0081150

von Stosch, H. A. 1973. Observations on vegetative reproduction and sexual life cycles of two freshwater dinoflagellates, *Gymondinium pseudopalustre* Schiller and *Woloszynskia apiculata* sp. nov. Br. Phycol. J. **8**: 105–134. doi:10.1080/00071617300650141

Yamaguchi, M., S. Itakura, I. Imai, and Y. Ishida. 1995. A rapid and precise technique for enumeration of resting cysts of *Alexandrium* spp. (Dinophyceae) in natural sediments. Phycologia **34**: 207–214. doi:10.2216/i0031-8884-34-3-207.1

Acknowledgments

Special thanks to Robert Olson for assistance in modification of the Imaging FlowCytobot, Micheil Boesel for technical assistance in the development of the observatory raft and its profiling winch, Heidi Sosik for assistance with image analysis, David Kulis, Madeline McKenna, Jennifer Haskell, and other staff and student members of the Anderson lab for assistance in collection and analysis of field samples, to Sophia Fox and Krista Lee (National Park Service) for nutrient analyses, and to other National Park Service staff at the Cape Cod National Seashore and Michael O'Connor, Dick Hilmer, and others at the Eastham Department of Natural Resources for assistance at the Salt Pond study site. This work was supported by the National Science Foundation (OCE-0430724, OCE-0911031, and OCE-1314642) and National Institutes of Health (NIEHS-1P50-ES021923-01) through the Woods Hole Center for Oceans and Human Health, MIT Sea Grant (NA14OAR4170077), Woods Hole Sea Grant (NA14OAR4170074, R/P-84), and National Park Service (NPS) Cooperative Agreement H238015504.

Conflict of Interest

None declared.

Submitted 10 January 2017
Revised 12 June 2017
Accepted 10 July 2017

Associate editor: Susanne Menden-Deuer